RADC-TDR-63-465, Vol. II
FINAL REPORT

INVESTIGATION OF NEW CONCEPTS FOR MICROWAVE POWER GENERATION (LASER STUDIES)

TECHNICAL DOCUMENTARY REPORT NO. RADC-TDR-63-465

December 1963

Techniques Branch
Rome Air Development Center
Research and Technology Division
Air Force Systems Command
Griffiss Air Force Base, New York

Project No.5573, Task No.557303

(Prepared under Contract No. AF30(602)-2833 by School of Electrical Engineering, Cornell University, Ithaca, New York)

ABSTRACT

An experimental and theoretical investigation of the emission of electrons, ions, and vertical particles from a tungsten cathode which is "surface-heated" by a laser beam is described. Principal emphasis is given the phenomenon of electron emission because of the interest in its application to the formation of a very dense electron beam. Two different experimental approaches are taken in obtaining electron emission. The first approach is to collect electrons which are "boiled off" the surface the laser beam strikes, while the second approach is to use a very thin tungsten ribbon to collect electrons from the surface opposite the one the laser beam strikes. Preliminary theoretical work describing these phenomena is discussed.

PUBLICATION REVIEW

This report has been reviewed and is approved. For further technical information on this project, contact Mr. R. Hunter Chilton, RALTE, Ext. 4251.

Approved: R. HUNTER CHILTON
Project Engineer
Directorate of Aerospace Surveillance & Control

Approved: ARTHUR J. FROHLICH
Chief, Techniques Laboratory
Directorate of Aerospace Surveillance & Control

FOR THE COMMANDER: IRVING J. GABELMAN
Director of Advanced Studies

AIR FORCE, Cato Show Ptg. Co. 12/31/63 - 264 -

CONTENTS

TECHNICAL REPORT

AN INVESTIGATION OF ELECTRON EMISSION FROM A TUNGSTEN SURFACE INDUCED BY A LASER BEAM

L. A. MacKenzie

I. INTRODUCTION

The objective of this study was an examination of the feasibility of obtaining a large electron emission per unit area from a cathode whose surface was heated to a high temperature with a laser light beam. The motivation for this study was the possibility of forming a small, relatively noiseless, and very dense electron beam, which would be useful in generating and amplifying high powers at millimeter frequencies. In addition, if an electron beam could be sufficiently well formed, the present upper frequency limit for linear beam millimeter-wave oscillators could be appreciably extended.

Two separate investigations of the thermionic emission obtained from metallic cathodes when surface heated with a laser beam were performed. One of these involved the heating of a thin strip of tungsten on one side and examining the emission obtained from the opposite side. The second investigation involved the heating of a tungsten cathode with a laser beam from one side and examing the emission obtained directly from the heated spot. A third class of experiments, which are presently in progress, is the examination of the photoemission obtained from a low work-function material illuminated by a laser beam. This work is directed specifically toward an understanding of the nonlinear quantum effect when one electron absorbs two photons to become a photoelectron.

In partial support of the experimental work involving thermionic emission, a classical theory of the heating effects at the cathode surface

was developed. This theory is sufficient to describe qualitatively the thermionic emission of electrons, but a more complete theory, which includes quantum effects, is required for a quantitative description of the emission and emission processes. This theory and the experimental work on the emission obtained directly from the heated spot on the cathode are described in a report included as an appendix.

II. PRELIMINARY STUDIES OF ELECTRON EMISSION FROM TUNGSTEN INDIRECTLY HEATED BY A PULSED LASER

G. C. Dalman

A. INTRODUCTION

This report is a summary of the results of some exploratory experiments* that were conducted to investigate the feasibility of obtaining very large electron-emission densities from a tungsten surface indirectly heated by a high-power, pulsed laser beam.

At Chiao Tung, indirectly heated tungsten surfaces were studied whereas directly heated surfaces were studied at Cornell. It was anticipated that since photons do not interact with the surface in the case of the indirectly heated surface, the electron emitting properties might be different from the directly heated case. A study of the indirectly heated case also seemed interesting from a practical point of view, since the electron optics and light optics can be readily separated.

Although the experiments performed were exploratory, they were successful in showing that under certain conditions very high current densities can be obtained with indirect heating of the cathode. Also

*These experiments were carried out by G. C. Dalman and T. S. Wen at the Institute of Electronics, Chiao Tung University, Taiwan, and by L. A. MacKenzie at Cornell University. The research at Taiwan was sponsored by the United Nations Special Fund, China Project (supervised by the International Telecommunications Union, Geneva, Switzerland) and the Institute of Electronics. The work at Cornell University was sponsored by Rome Air Development Center under Contract No. AF30(602)-2833, "Investigation of New Concepts for Microwave Power Generation."

some emitting properties were observed to be different from those in the directly heated cathode.

The sections that follow give a description of the experimental equipment used, a discussion of the results obtained, and the conclusions derived from this study. Suggestions for further study are also included.

B. EXPERIMENTAL APPARATUS

The experimental apparatus used is shown schematically in Figure 2.1. It consisted of a pulsed-operated ruby laser, a parallel-plane diode, which had a tungsten-ribbon anode and cathode and was continuously evacuated by a VacIon pump, a laser output sampler, a Tektronix dual-trace oscilloscope for simultaneously viewing the laser output and the diode current, and a simple lens for focusing the laser beam on the cathode to a diameter of about 0.005 in. to 0.010 in.

The test diode, shown in greater detail in Figure 2.2, consisted of two crossed tungsten ribbons 0.015-in. wide and 0.0005-in. thick, which were spring loaded and spaced approximately 0.001 in. apart. The diode power supply used had an equivalent circuit corresponding to that of Figure 2.3. It is clear that this would allow measurement only of the peak values of the emission, but this was found to be necessary to prevent the burning out of the thin anode ribbon. During all the measurements, the residual diode pressure was in the 10^{-6} Torr range. No increase in pressure was observed when the laser pulse illuminated the diode.

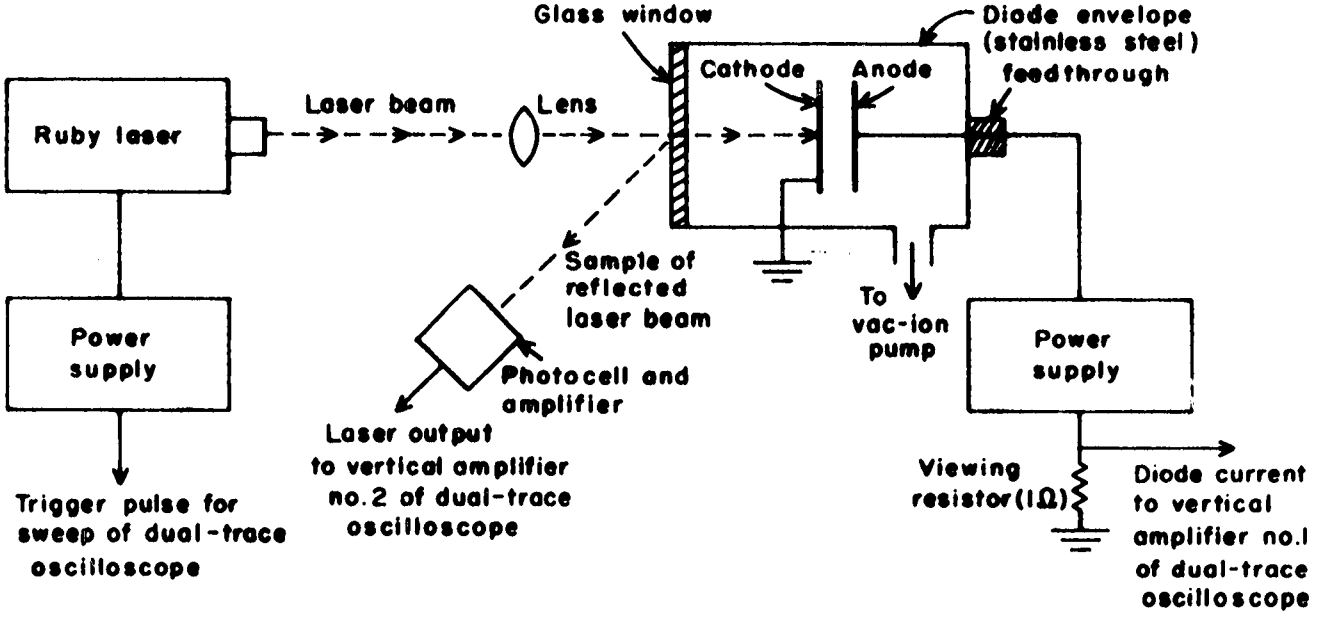

FIGURE 2.1. Schematic Diagram of Experimental Equipment.

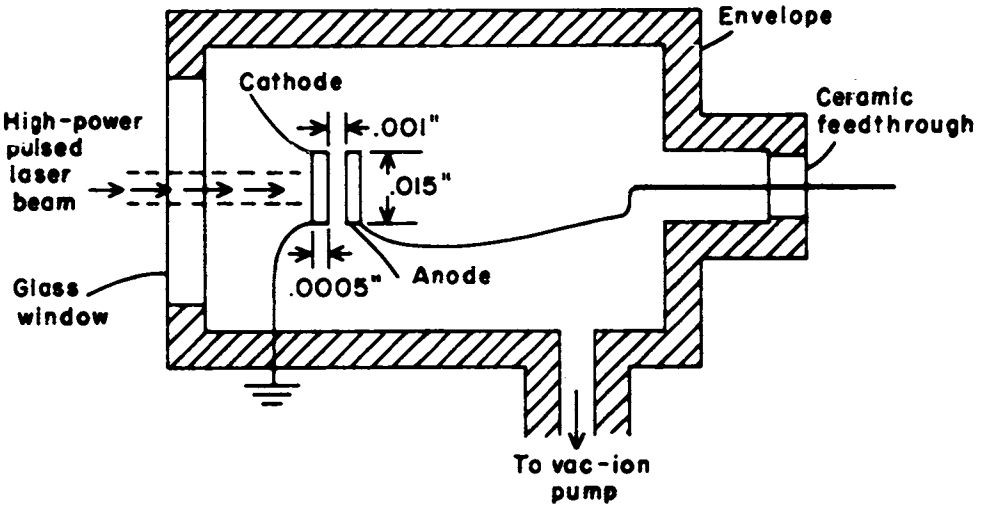

FIGURE 2.2. Indirectly Heated Parallel-Plane Diode

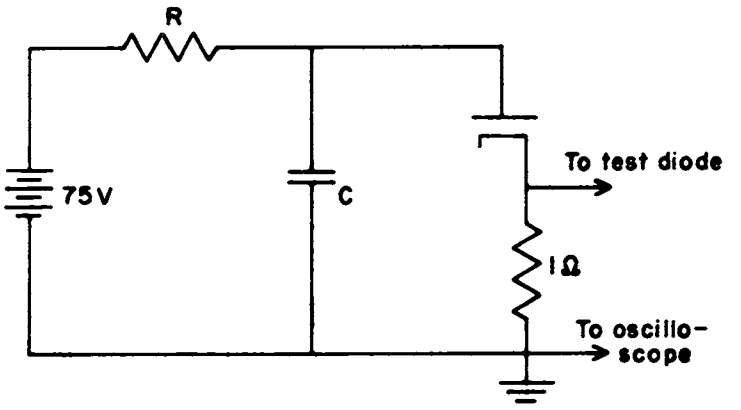

FIGURE 2.3. Peak-Emission Test Circuit.

The ruby laser was identical to that used at Cornell University for the laser-induced electron emission research,[1,2] except that a ruby crystal with dielectric coated ends was used, whereas the one used at Cornell had chiseled ends and no coating. To prevent burning out of the end coatings, the laser had to be operated close to the threshold value. It was found that the laser output was less spiked than the output of the Cornell laser and considerably lower in power output. Fortunately, because of the small mass of the tungsten ribbon, adequate power was available to heat the tungsten to temperatures close to its melting point.

C. EXPERIMENTAL RESULTS

The pulsed laser beam was directed on the cathode and a voltage of between 50v and 100v was applied. It was found that currents very much in excess of the anticipated values were obtained, but it was observed that after repeated pulses (about 5 or 10 pulses at a rate of one per minute) the emission decayed to a very small value. It was also found, however, that the emission recovered when the diode was allowed to remain inoperative for a period of 15 minutes or longer.

The very high initial peak currents were of the greatest interest in this study; therefore, after complete recovery of the diode, the peak-current output was recorded photographically. A typical result is shown in Figure 2.4 along with the sampled laser output pulse. No measure of the power output of the laser was available, but it was

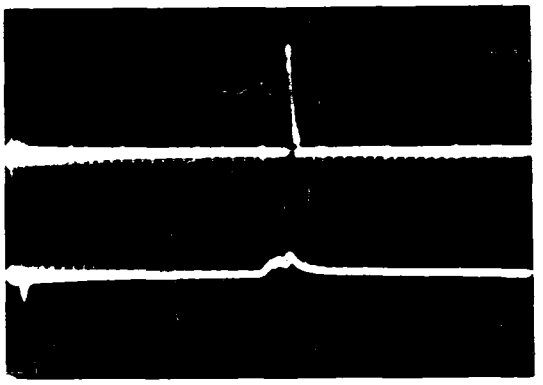

FIGURE 2.4. Top: Diode Current (25 a peak), Pulse Duration about 20 μs. Pulse Starts about 60 μs after Application of Laser Pulse. Bottom: Sample of Laser Pulse, Pulse Duration about 100 μs.

probably of the order of 0.1 joules per pulse. The peak current was 25 a with an anode voltage of 75 v. Increasing the voltage to 100 v did not increase the diode current measurably, but decreasing it below 50 v did decrease it. Reversing the polarity of the diode voltage resulted in no measurable current.

These measurements were made repeatedly and were fairly consistent. An attempt to increase the duration of the anode voltage pulse (by placing capacitors across the diode) failed because of the increased dissipation at the anode, which caused it to burn out.

D. DISCUSSION

The measured current peak of the diode greatly exceeded the expected value. A theoretical study[3] of the temperature distribution (both of the heating and cooling processes) of a tungsten ribbon irradiated by a laser pulse showed that only a very narrow strip of the ribbon could be heated close to the melting point, assuming that the ribbon was illuminated over its entire width and over a length equal to the width. Because of end cooling, the temperature dropped off rapidly to values too cool to emit a significant amount of current. If we assume, optimistically, that a 0.005 in. x 0.015 in. rectangular strip were heated, then the theoretical value of the zero-field emission available would be 0.23a, where the emission current density of the melting point is assumed to be 480 a/cm^2. Thus, pulsed currents were observed of about two orders of magnitude greater than those predicted by the simplified calculation.

At this time, we can only speculate as to the reasons for the large currents observed. One possibility is that adsorbed gases on the surface of the tungsten are released when the surface temperature rises. Then when, as a result of thermionic emission, electrons start to flow, the gas is ionized and produces a plasma sheath adjacent to the heated portion of the cathode. Thus, very high fields are produced at the hot tungsten surface and, as a result, the field emission effects cause a further increase in current. Or some of these ions might be evaporated tungsten. A further reason for the high currents observed

might be that the surface of the tungsten might actually be heated beyond the melting point; or a dipole layer might exist on the emitting surface, which lowers its effective work function. The hypothesis that ions are present is clearly valid, since the space-charge-limited current for an anode voltage of 75 v is in the milliampere rather than ampere range, but many more fundamental experimental studies must be conducted before the basic reasons for the large currents observed are understood.

It is interesting at this point to calculate the electron plasma frequency and the electron density. For the plasma frequency, we have

$$f_p = 2900 \frac{J^{1/2}}{V^{1/4}} \quad ,$$

where J is in amperes per square centimeter, V is in volts, and f_p is in megacycles per second. If we assume an operation where $J = 40 \times 10^3$ and $V = 100$, then the plasma frequency is 183 Gc/s, a value far in excess of the values found in conventional electron devices.

For an estimate of the electron density at the anode plane, let us first calculate the electron space-charge density at the anode. We have

$$\rho = \frac{J}{59.32\, V^{1/2}} \quad \text{coul/M}^2$$

so that $\rho \approx 6.75 \times 10^{-3}$ coul/M^2 and the electron density n is 4.2×10^{10} electrons/cm^3.

E. CONCLUSIONS AND SUGGESTIONS FOR FURTHER STUDY

These preliminary studies have shown that:

1. It is possible to obtain electron current densities as high as about 40×10^3 a/cm^2.

2. A pulsed plasma can be produced with electron densities of the order of 10^{10} electrons/cm^3 and with plasma frequencies of about 180 Gc/s .

3. The high-pulse emission appears to be available for short periods only, requiring an interval of about fifteen minutes between periods of repeated pulses.

These results are of considerable interest, since the properties of beams with high plasma frequencies, plasmas with high electron densities, and beams with high-power densities can be studied, even if only on a pulse basis. These studies should be undertaken because they should help establish the ultimate capabilities of beam devices in the very high-power density range and in the millimeter-wavelength range; and because interesting microwave properties of plasma having plasma frequencies in the high microwave range can be investigated in a relatively easy manner. Parallel with these studies, a more carefully controlled study of the pulsed emission properties of tungsten and other materials should be carried out to try to explain the phenomena observed and to develop techniques to control the emission and increase the stability of the emitting surface.

F. REFERENCES

1. B. W. Woodward and G. J. Wolga, "Fabrication of High-Efficiency Laser Cavities," Rev. Sci. Inst., 33 (1962), pp. 1463-1465.

2. G. J. Wolga and C. A. Waterstrat, "Improved Procedure for Fabrication of High-Efficiency Laser Cavities," submitted to Rev. Sci. Inst. for publication.

3. Mao-Chieh Chen, "Analysis of the Electron Emission from a Tungsten Surface Indirectly Heated by a Laser Pulse," M. S. thesis, Chiao Tung University, Hsinchu, Taiwan (June 1963).

III. NOTE ON ELECTRON AND ION EMISSION FROM LASER-HEATED OXIDE CATHODES

G. C. Dalman

An exploratory study* of the emission of electrons and ions from a cold oxide cathode surface was made to assess the usefulness of the conventional oxide cathode as a high-density current source.

Figure 3.1 shows a schematic diagram of the tube structure used in this study. The tube is a commercial 6J6 double triode with an oxide-coated cathode. Two regions (shown in Figure 3.1) of the

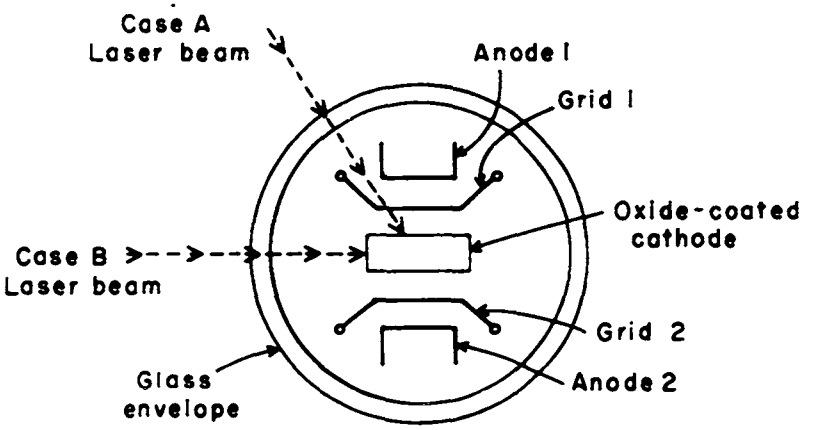

FIGURE 3.1. Schematic Diagram of Miniature Glass 6J6 Double Triode Showing the Two Regions of Cathode that Were Irradiated by Pulsed Laser Beam.

---

* See footnote at beginning of Chapter II.

cathode were irradiated. In Case A, the light beam was directed through the grid wires on the cathode coating; in Case B, the light was directed on the side of the coated cathode. Figures 3.2a, b, and c are the circuits used to measure the currents for the two cases shown in Figure 3.1.

Figure 3.3 is the result observed at Chiao Tung for Case A in which the pulsed laser light was directed through the grid wires. In the experiment the laser output was made as small as possible so as to avoid overheating the cathode coating. The cathode current was observed during the pulse using the circuit of Figure 3.2a. Peak currents of approximately 100 ma were obtained with a wave form which followed that of the laser output. It is believed that in this case the current is due to both thermionic and photoemission, but it was not possible to separate the two currents in the measurement.

At Cornell a similar experiment was performed using the circuit of Figure 3.2c. In this case the side of the cathode was radiated as illustrated in Figure 3.1, Case B. The results obtained, shown in Figure 3.4, are the same as those of Figure 3.3. For the result shown in Figure 3.5, however, the laser output was slightly higher. In this case a d-c component appeared in the measured cathode current. It is believed that this added component of current is due to thermionic emission resulting from the temperature of the locally heated coating rising above the emitting temperature (i.e., above about 750°C).

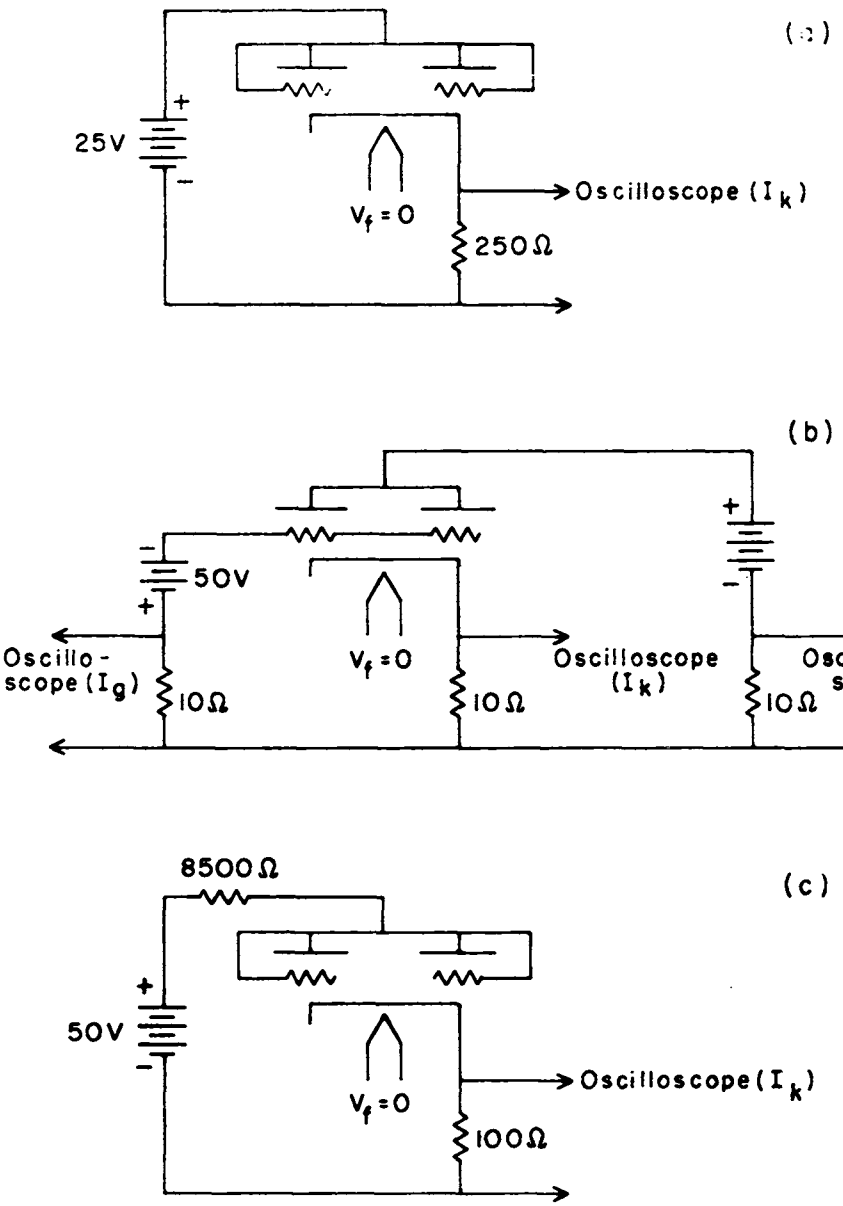

FIGURE [illegible] Schematic Diagrams of Circuits (a) Case A, Diode Measurement; (b) Case A, Triode Measurement; (c) Case B, Diode Measurement.

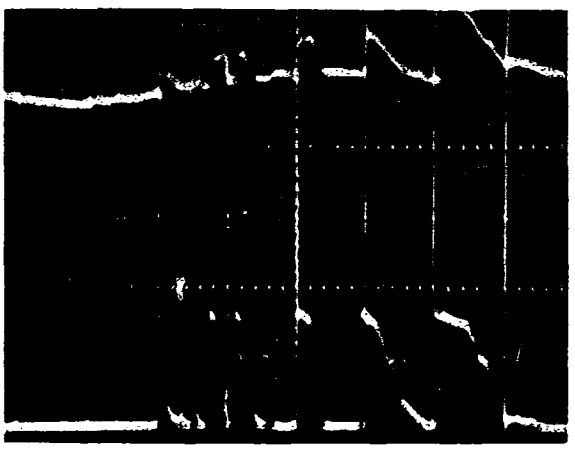

FIGURE 3.3. Laser Output (Top) and Cathode Current (Bottom) Observed on an Oxide Cathode Which Was Initially at Room Temperature (Results Obtained at Chiao Tung University).

Both at Chiao Tung and Cornell several tubes were tested in this manner and it was found, in all cases, that the coating gradually disappeared in the radiated regions and the tubes ultimately became gassy. It is believed that the coating is thermally evaporated and dissociates into barium ions (positive) and oxygen ions (negative). This idea was studied briefly at Chiao Tung using the circuit of Figure 3.2b. From the figure it is clear that the positive ions produced are collected by the grid and the electrons and the negative ions produced are collected at the anode.

In this experiment the laser output was increased over that of the previous tests to accentuate the effects of the evaporation of the

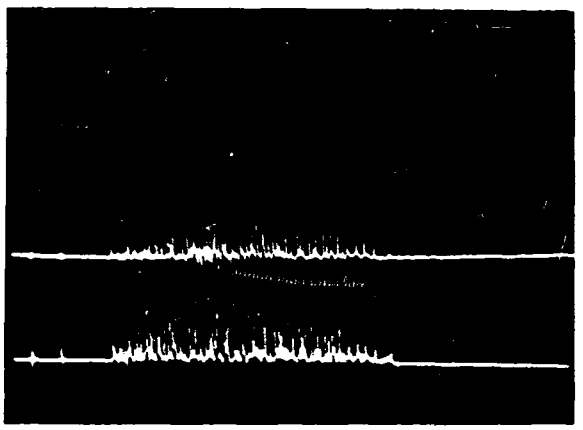

FIGURE 3.4. Laser Output (Bottom) and Cathode Current (Top) Observed on an Oxide Cathode Which Was Initially at Room Temperature (Results Obtained at Cornell University).

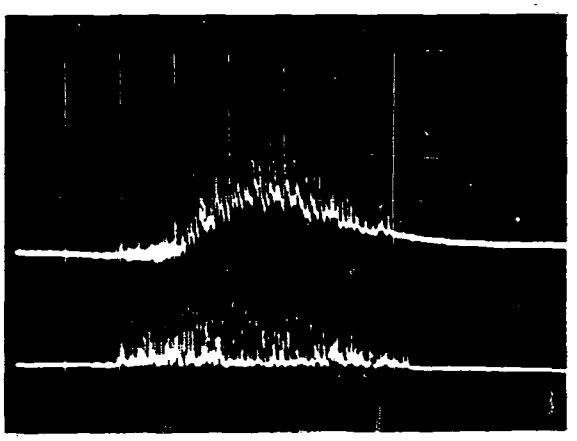

FIGURE 3.5. As in Figure 3.4, but with a Slightly Larger Laser Power Output (Results Obtained at Cornell University).

coating. Figure 3.6 shows a typical result. The two top curves and the two bottom curves were measured simultaneously on a dual-beam oscilloscope. It was found in other similar experiments that the leading edges of the cathode current, plate current and grid current pulses always occurred at the same time. Therefore two separate photographs were lined up as shown in order to represent approximately the actual results that were obtained.

Initially the tube was cut off so that no current flowed during the first 20 μs or 30 μs of the test. After that time the coating

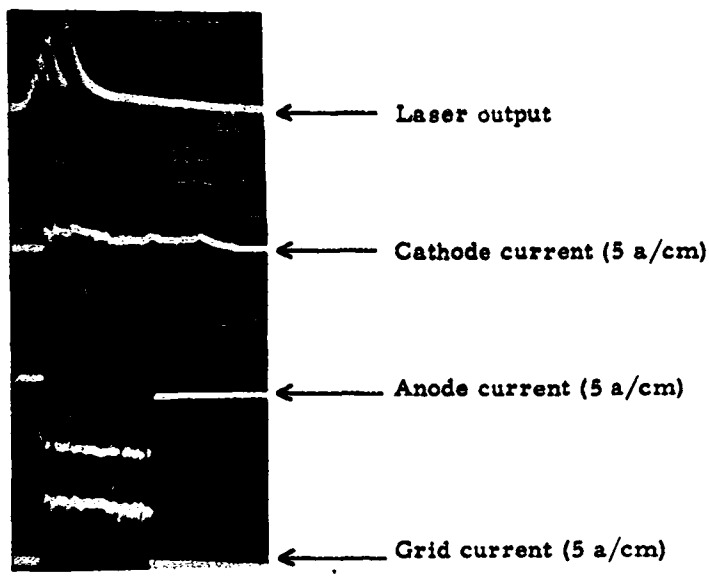

Time scale: 50 μs/cm

FIGURE 3.6. Laser Output and Cathode Current (Measured Simultaneously) Combined with Plate Current and Grid Current (Measured Simultaneously) for Triode with Laser Irradiated Cathode Which Was Initially at Room Temperature.

appeared to dissociate, and a large positive ion current (barium ions) flowed to the grid and a large current was collected by the anode (negative oxygen ions and electrons). The cathode current had to equal the electron-current component of the flow since the ions were assumed to be formed at the cathode surface. When the laser output dropped below the temperature at which the coating could dissociate thermally, the ion current stopped abruptly. Interestingly, the cathode current continued even though the tube was cut off. It is believed to be a result of a sharp rise in the residual gas pressure.

As a source of very high current electron emission, a laser-radiated oxide-coated cathode does not seem practical, since the coating breaks down readily. Advantage, however, may be taken of this effect to produce a pulsed source of high-density positive or negative ions.

IV. DOUBLE-QUANTUM PHOTOELECTRIC EMISSION

G. Wolga and H. Bowers

Considerable effort has gone into a theoretical study of double photon-induced photoelectric emission from metallic single crystals as well as consideration and design of an experiment to observe such emission. The double-photon absorption process leading to this photo electric emission is a second-order process in the conventional perturbation treatment of the interaction of free, metallic electrons with electromagnetic radiation and is usually very improbable. It proves necessary, therefore, to use a ruby laser as a source of light in order to obtain the high fields necessary to produce this emission in measurable quantities. Distinguishing this second-order photo-electric emisssion from simultaneously occurring thermionic emission resulting from heating of the crystal by intense light necessitated a fairly detailed study of some of the aspects of thermionic emission. These studies revealed that a high-frequency modulation of the laser light impinging on the crystal might well make the second-order effect observable. The quantum mechanical effects of this modulation on the second-order photo effect were studied in detail along with the thermi-onic emission response to this modulation. The modulation itself will be accomplished by means of the longitudinal Pockel's effect in KDP. The details of this study will be described in a later report, and are only summarized here.

A. DESCRIPTION OF APPARATUS

The physical setup of the experimental apparatus is shown in Figure 4.1. The crystal to be studied and the electrode that collects either the electrons or the ions emitted from the crystal are contained in a vacuum system capable of attaining pressures of the order of 10^{-9} - 10^{-10} Torr . The pressure actually attained will be somewhat limited by the vapor pressure of the material used in the experiment. The crystal can be rotated by means of a rotating mechanical feedthrough to the vacuum systems. The collector has a hole in it and is placed in front of the crystal in such a way that light from the laser entering the vacuum system through a glass window can pass through this hole and impinge on the crystal. Calculations show that the space-charge effects of this diode on the photoelectric experiment should be negligible.

Since the laser utilizes a 90° ruby rod, the light emitted is linearly polarized in a specific direction normal to the direction of propagation. The amount that the angle of polarization of the light passing through the KDP is rotated depends on the voltage applied to the KDP. The light then passes through a polaroid filter, and the intensity of the light passing through the filter will, of course, depend on the angle of polarization. Thus by modulating the voltage applied to the KDP crystal, it is possible to modulate the intensity of the laser beam. The response of the double quantum photoemission to an amplitude-modulated light beam has been calculated. By means of a telescope and lens, the light can be focused to various spot sizes on the crystal in the vacuum system.

The circuit for measuring the current emitted from the crystal is shown in Figure 4.2. When the switch is in position 1, the collector is negative and ion current is measured. The cathode follower is used to match the impedance of this circuit to the impedance of the coaxial transmission line leading to the oscilloscope. This circuit is enclosed in a copper box and is located physically close to the vacuum system in order to minimize noise pickup.

B. SECOND-ORDER PHOTOELECTRIC EFFECT

An expression has been derived[1] for the second-order photoelectric current,* which can be written as

$$j = A\,(\gamma_o + \gamma_f)\,\frac{\gamma_o^3}{\gamma^8}\,I\,E_o^4\,\sin^4\theta \quad , \tag{4.1}$$

where

j = current in a/m^2 ,

γ_o = W_o/h ,

γ_f = W_f/h ,

γ = light frequency ,

W_o = work function ,

W_f = Fermi energy ,

E_o = electric field strength of the light ,

*Errors in this calculation were corrected in the present work.

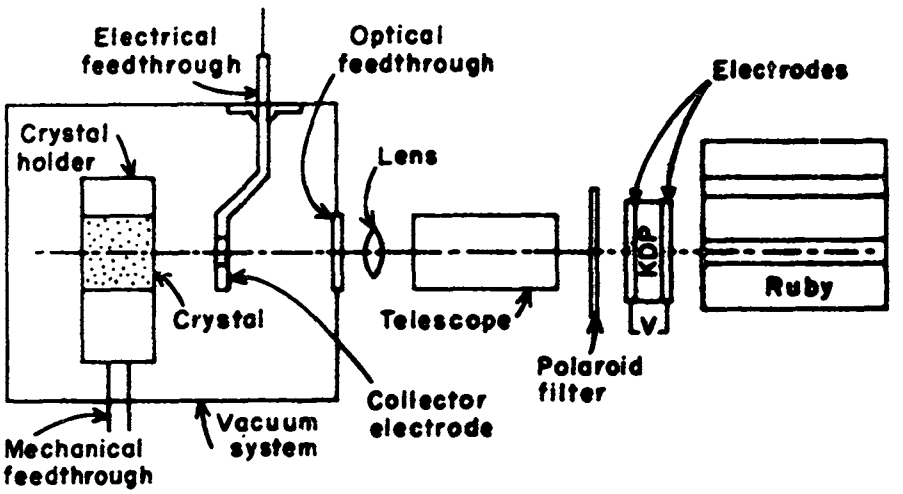

FIGURE 4.1. Vacuum and Laser System for Emission Studies.

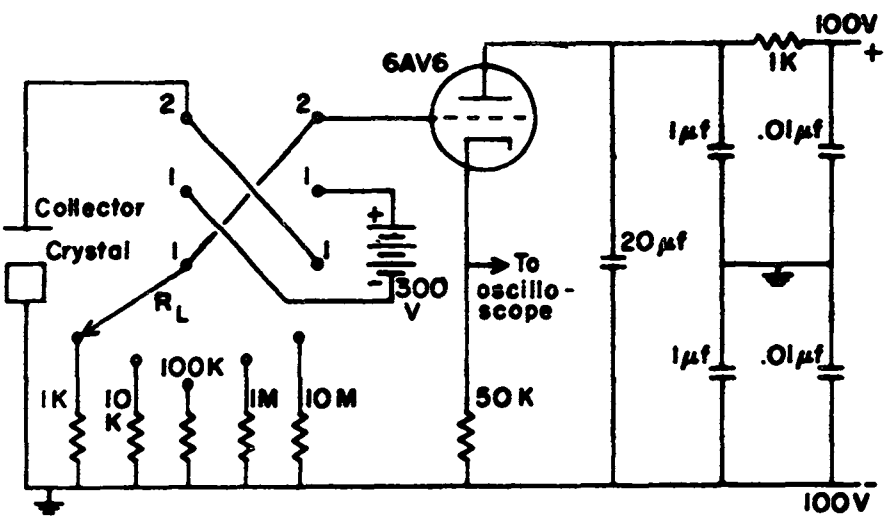

FIGURE 4.2. Vacuum Diode Electrical Circuit.

θ = angle of incidence with respect to the normal of the crystal face.

$A = 3.96 \times 10^{32}$ mks units and

$$I = \int_0^{\sqrt{\mu-1}} d\lambda \, (\mu - 1 - \lambda^2)\,(\lambda^2 + 2\eta - \mu)^{\frac{1}{2}}\, \lambda^2 \quad ,$$

$$\cdot \left\{ \frac{\frac{s}{2}\mu L \eta + 2\left[(\eta+\lambda^2)\,(2\eta+\lambda^2)\right]^{\frac{1}{2}} + 2\left[(\mu-\lambda^2)(\mu-\eta-\lambda^2)\right]^{\frac{1}{2}}}{4\eta - \mu - 2\lambda^4 + 2\left[(2\eta+d^2)(2\eta-\mu-\lambda^2)\right]^{\frac{1}{2}}} \right\} ,$$

where

$$\eta = \frac{\gamma}{\gamma_o} \quad ,$$

$$\mu = \frac{\gamma_o + \gamma_f}{\gamma_o} \quad .$$

Values of I and $j/E_o^4 \sin^4\theta$ have been calculated for various materials, and these results are given in Table 1. The table includes the values of the work function and Fermi level used in the calculations. Since the light from a ruby laser has an electric field strength on the order of $10^5 - 10^6$ V/m , it is conceivable that second-order photo currents may be observable.

There will be present at the same time, however, a certain amount of thermionic emission as a result of the heating of the crystal by the laser. This emission may well be as large or larger than the photoelectric current. Since the photoelectric current is proportional

to E^4, modulation of the light should yield a modulation of the photoelectric current. If the temperature of the crystal does not respond to such modulation, then the photoelectric current should be distinguishable from the thermionic emission.

If the heat input to the surface of a crystal is varying at a frequency ω, then linear heat-flow theory predicts that the temperature at some point on the crystal will also fluctuate at a frequency ω, and that the amplitude of this fluctuation will be attenuated at higher frequencies. It might therefore be expected that the temperature of a crystal will not respond to a sufficiently high frequency modulation of the light input to the crystal.

C. EXPERIMENTAL RESULTS

Zinc was chosen for most of the experimental work reported here because large single crystals are easily obtained, and zinc is the easiest metal to work with from among those listed in Table I.

Thermionic emission from a large zinc crystal heated by both focused and unfocused ruby-laser radiation has been observed. The focused laser beam produces a spiking thermionic current similar in characteristics to the current obtained with tungsten and described in preceding chapters. Experiments with low-intensity, unfocused laser beams have been difficult to interpret, since the very small thermionic currents obtained require a high-load resistor to achieve sufficient sensitivity, and the frequency response of the circuit is impaired by the resultant large time constant. We are still pursuing the problem

TABLE I

	W_o (ev)	W_f (ev)	I	$j/E^4 \sin^4\theta$ (a/v^4m^2)
B_a	2.48	2.26	.042	3.43×10^{-27}
C_a	2.71	2.99	.024	3.06×10^{-27}
C_e	2.84	3.43	.015	2.49×10^{-27}
K	2.24	2.04	.077	4.13×10^{-27}
N_a	2.28	3.12	.097	6.95×10^{-27}
R_b	2.09	1.79	.098	3.89×10^{-27}
Sr	2.74	2.51	.019	2.33×10^{-27}
Z_η	3.5	5.95	4.5×10^{-5}	2×10^{-30}

of designing circuitry that can accommodate load resistors as high as 10^7 ohms without degrading frequency response. Since the ratio of photo to thermionic emission improves at low intensities of illumination, it will be important to work with unfocused laser beams.

It has been possible, by reversing the polarity on the collector, to observe ion current as well as electron (from zinc) current when the laser was focused. For a given energy input to the crystal, the ion current was of the same order of magnitude as the electron current and had approximately the same characteristics. The pressure in the diode had been $1\text{-}5 \times 10^{-9}$ Torr during all the experiments. A momentary rise in pressure, however, was observed while the laser pulse was striking the crystal. This is believed to originate either from a vaporization of the target material or from absorbed

gases on the surface and might be linked to the ion current observed.

The thermionic emission as a function of the angle of incidence of the laser beam to the surface was studied theoretically. The angular variation is important because thermionic emission is maximum at normal incidence, while photoemission is minimum at normal incidence. Calculations show that thermionic emission will fall off away from normal incidence while photoemission will be at a maximum when the laser beam strikes the crystal surface at an angle of 60° to the normal of the crystal surface. Therefore, the angular variation of the emission may be used to discriminate between thermionic and photoemission. We are planning to measure the angular response of the thermionic emission and to check it with our calculations.

Various methods for suppressing thermionic emission are also being considered. One such method could be to cool the crystal and maintain good thermal contact with a cold heat sink during the laser pulse. Double quantum photoemission with a low work function material would be relatively unaffected if the material were cooled in this manner.

At present no attempt has been made to modulate the laser beam or to observe photoelectric emission, since it is felt that a better understanding of laser-induced thermionic emission is necessary before observation of double-quantum photoelectric emission is attempted.

D. REFERENCES

1. Richard L. Smith, "Two-Photon Photoelectric Effect," Phys. Rev., 128 (1962), p. 2225.

AN INVESTIGATION OF ELECTRON EMISSION FROM A TUNGSTEN SURFACE INDUCED BY A LASER BEAM

L. A. MacKenzie

CONTENTS

ABSTRACT

The emission of electrons and ions from a metallic cathode when the surface is heated by a pulsed laser beam was investigated experimentally. The incident energy of the laser beam on the cathode ranged from 0.1 joules to 3 joules over a 300-μs pulse. A very large electron emission density was found under ordinary thermionic emission conditions. Also, a plasma discharge was obtained, which contained a large volumetric electron density. Some initial theoretical work is described as support for the experiments reported.

I. INTRODUCTION

This report describes the theoretical and experimental work performed in obtaining the emission of electrons, ions, and neutral particles from a metallic cathode, when it was surface heated with a focused laser beam. The tungsten cathodes were designed to yield particle emission directly from the spot illuminated by the laser beam. A classical, linearized theory is presented, which describes this emission qualitatively.

II. THEORY OF LASER-STIMULATED THERMIONIC EMISSION

It is possible to formulate a rather simple theory of the thermionic emission of electrons induced by a laser beam from a metallic cathode. Even though there are some serious omissions in this theory, it will qualitatively describe some of the emission characteristics observed experimentally. This simple theory and some of the conclusions derived from it follow.

A. LIGHT ABSORPTION BY CATHODE MATERIAL

If a light beam is incident upon the plane face of a metallic cathode, part of this beam is reflected and part is transmitted through the material. If the material is a good conductor, the transmitted light beam will be absorbed in a thin layer of the material near the surface. Since the light beam of interest is from a laser, and hence preferentially polarized, the absorption characteristics may be readily estimated by a classical treatment. The light beam may be considered as a plane electromagnetic wave, normally incident on the metallic surface, and the cathode material may be considered perfectly homogeneous. This viewpoint obviously ignores the lattice structure of the cathode and any imperfections in this lattice. Consider the metallic material to be semi-infinite, so that there is only one interface for the light beam to cross. The

reflection and absorption characteristics at this interface may then be simply calculated by solving Maxwell's equations, subject to the boundary conditions that the tangential components of the electric and magnetic fields are continous across the boundary. In terms of the complex refractive index n_c, these equations become:

$$\underline{\nabla} \times \underline{E} = - j\omega\mu \underline{H} \quad , \tag{1}$$

$$\underline{\nabla} \times \underline{H} = j\omega \epsilon_o n_c^2 \underline{E} \quad , \tag{2}$$

$$\underline{\nabla} \cdot n_c^2 \underline{E} = 0 \quad , \tag{3}$$

$$\underline{\nabla} \cdot \underline{H} = 0 \quad , \tag{4}$$

where

$$n_c^2 = \frac{\epsilon}{\epsilon_o} \left(1 - j \frac{\sigma}{\omega\epsilon}\right) \quad , \tag{5}$$

and $e^{j\omega t}$ time variations are assumed. A little algebra shows that the transmitted power density P_t at a distance z from the interface is related to the incident power density P_i as follows:

$$P_t = \frac{4 \, \mathrm{Re}\,(n_c)}{\left|1 + n_c\right|^2} \, e^{+ 2kz \, I_m (n_c)} \, P_i \quad , \tag{6}$$

where n_c is the complex refractive index for the metallic cathode. If we let

$$A = \sqrt{\frac{\sigma}{2\omega\epsilon}} \quad , \tag{7}$$

then Equation (6) becomes, approximately,

$$P_t = P_i \frac{2}{A} e^{-2kAz} \quad . \tag{8}$$

The average power density absorbed per unit depth P_a in the metallic cathode is readily found by

$$P_a = - \frac{dP_t}{dz} = P_i 4ke^{-2kAz} \quad . \tag{9}$$

If we denote the transmitted power at the interface $z = o$ by P_{to}, then

$$P_a = \alpha P_{to} e^{-\alpha z} \quad , \tag{10}$$

where

$$\alpha = 2kA \quad . \tag{11}$$

Equation (10) describes the average power density absorbed per unit depth in the cathode material in terms of the power density transmitted across the interface for normal incidence. The characteristic absorption depth or "skin" depth is very small, being approximately 86 A° for tungsten, if the low-frequency conductivity is used and the wavelength of light is 7000 Å. It is the absorption of this light energy that heats the cathode material to a high temperature, particularly at and near the surface. It should be observed that this calculation does not account for a change in the conductivity of the cathode material as the temperature changes. This means that

Equation (10) may be used as it stands, except that if P_{to} is a function of time, then α should also be a function of time.

The solution in this section for the power absorbed in the cathode material is valid for normal incidence of a laser light beam on a plane surface. The extension to oblique incidence is obvious.

B. GENERAL SOLUTION FOR SURFACE TEMPERATURE OF A SEMI-INFINITE MEDIUM

A classical solution for the surface temperature of a block of material heated with a laser beam may be obtained from the heat equation,

$$\nabla^2 T(\underline{r}, t) - \frac{\rho C_v}{K} \frac{\partial T(\underline{r}, t)}{\partial t} - \frac{1}{C^2} \frac{\partial^2 T(\underline{r}, t)}{\partial t^2} = \frac{-Q(\underline{r}, t)}{K} , \qquad (12)$$

where

$T(\underline{r}, t)$ = the absolute temperature as a function of space and time,

$Q(\underline{r}, t)$ = any heat source as a function of space and time,

K = the thermal conductivity of the material,

c_v = the heat capacity of the material,

ρ = the density of the material, and

c = the velocity of sound in the material.

All of the coefficients of Equation (12) are properly functions of the temperature, so that this equation is nonlinear. Since Equation (12)

will be used to describe the thermionic emission of electrons from the metallic surface qualitatively, and since a quantum mechanical approach is probably required for a detailed quantitative description, it is not worth while to solve Equation (12) in its nonlinear form. Consequently, a linearized version of this equation is used, in which the parameters are evaluated at room temperature. Also since the area of the illuminated spot on the metallic cathode is much larger than the "skin" depth, a one-dimensional model is chosen, in which transverse variations are neglected. Finally, it is convenient to consider first a semi-infinite cathode, even though this introduces some minor complications, as will be shown in a later section. The model described is shown in Figure 1.

From Equation (10), the heat equation for this simple model becomes

$$\frac{\partial^2}{\partial z^2} T(z,t) - \frac{\rho c_v}{K} \frac{\partial T(z,t)}{\partial t} - \frac{1}{C^2} \frac{\partial^2 T(z,t)}{\partial t^2} = - \frac{a}{K} P_{to}(t)\, e^{-az} . \tag{13}$$

The final simplification comes by neglecting the finite propagation of heat energy in the medium. Since most events of interest occur at and near the surface, the slight time delay is not significant, and its omission is not serious. For convenience, define

$$a = \frac{K}{\rho c_v} , \tag{14}$$

and

$$\beta = a\alpha^2 \quad . \tag{15}$$

Then the final form of Equation (12) that we consider is

$$\frac{\partial^2 T(z,t)}{\partial z^2} - \frac{1}{a}\frac{\partial T(z,t)}{\partial t} = -\frac{\alpha}{K} P_{to}(t)\, e^{-\alpha z} \quad . \tag{16}$$

The boundary and initial conditions to be used are as follows:

(1) the initial temperature is zero or this may equally well be a constant (room temperature), i.e.,

$$T(z,o) = 0 \quad ; \tag{17}$$

(2) no temperature rise is experienced at the far end of the medium, which is infinitely far from the light beam, i.e.,

$$T(\infty, t) = \lim_{z\to\infty} T(z,t) = 0 \quad ; \tag{18}$$

(3) the temperature gradient or heat flow at the interface matches that resulting from the transmitted light beam, i.e.,

$$\frac{\partial T}{\partial z}(o,t) = -\frac{1}{K} P_{to}(t) \quad . \tag{19}$$

It should be observed that the last boundary condition neglects energy loss by radiation from the hot interface. The consequences of this approximation are examined in a later section.

The approach to the solution for Equation (16) is to take the Laplace transform with respect to the time variable, solve the resulting ordinary differential equation, and express the resulting temperature, which is a function of space and time as a convolution integral. Once one specifies a particular time variation for $P_{to}(t)$, an evaluation of this integral will yield the desired temperature function. Let

$$\tau(z,p) = \mathcal{L}[T(z,t)] = \int_0^\infty e^{-pt}\, T(z,t)\, dt; \tag{20}$$

then, Equation (16) becomes

$$\frac{\partial^2}{\partial z^2}\, \tau(z,p) - \frac{p}{a}\, \tau(z,p) = -\frac{a}{K}\, F(p)\, e^{-az} \quad , \tag{21}$$

where

$$F(p) = \mathcal{L}[P_{to}(t)] \quad . \tag{22}$$

The solution of Equation (21) subject to the boundary conditions on z is

$$\tau(z,p) = \frac{\beta}{aK}\, \frac{F(p)}{(\beta - p)} \left[\sqrt{\frac{\beta}{p}}\, e^{-\sqrt{\frac{p}{a}}\, z} - e^{-az} \right] + \frac{F(p)}{aK} \sqrt{\frac{\beta}{p}}\, e^{-\sqrt{\frac{p}{a}}\, z} \quad . \tag{23}$$

The resulting temperature variation is readily found from the convolution integral,

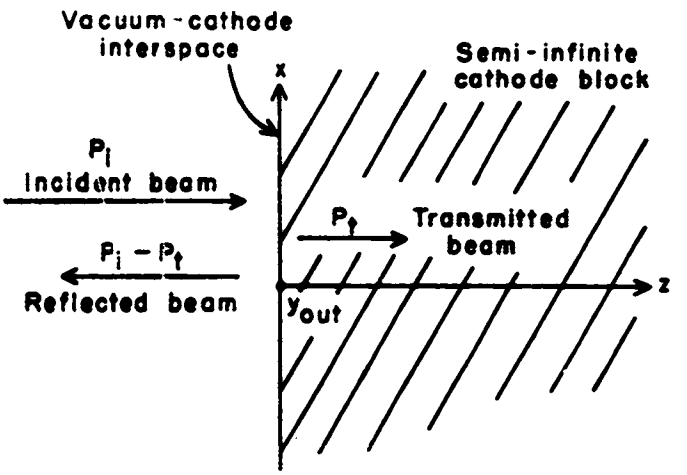

FIGURE 1. Model for Classical Temperature Calculation.

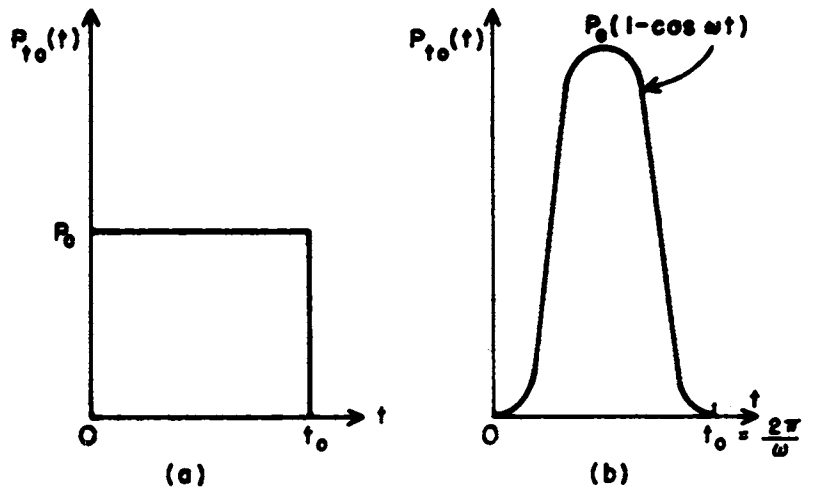

FIGURE 2. Assumed Forms for Laser Light Pulse.

$$T(z,t) = \frac{\beta}{\alpha K} \int_0^t P_{to}\,(t-x)\, g(z,x)\, dx \qquad (24)$$

where $g(z,x)$ is the inverse Laplace transform of the appropriate part of Equation (23), that is,

$$g(z,t) = e^{-\alpha z+\beta t} + \frac{e}{\Sigma}^{\alpha z+\beta t} \quad \mathrm{Erfc}\left(\frac{\alpha z}{2\sqrt{\beta t}} + \sqrt{\beta t}\right)$$

$$- \frac{e}{\Sigma}^{-\alpha z+\beta t} \quad \mathrm{Erfc}\left(\frac{\alpha z}{2\sqrt{\beta t}} - \sqrt{\beta t}\right) + \frac{e^{\frac{-(\alpha z)^2}{4\beta t}}}{\sqrt{\pi\beta t}} \quad . \qquad (25)$$

The function denoted by "Erfc" is the complementary error function.

A special case of interest is the temperature at the interface $z = 0$ as a function of time. For this case the kernel in Equation (24) has the simple form,

$$g(o,t) = e^{\beta t} \quad \mathrm{Erfc}\left(\sqrt{\beta t}\right) + \frac{1}{\sqrt{\pi\beta t}} \qquad (26)$$

Next, it is of interest to consider the application of these results to specific types of functions for $P_{to}(t)$, i.e., specific shapes of the pulsed laser beam. These solutions are performed in Section C, and numerical results are considered in Section D.

C. SPECIFIC FORMS FOR LASER LIGHT PULSE

We consider two special cases for the envelop of the laser light pulse. The first (Case 1) is a rectangular laser pulse chosen because the resulting convolution integral is simple to evaluate. The second (Case 2) is a $\sin^2$ pulse, which is a convenient analytical form for a laser pulse that is smooth but of finite length. These pulses are shown in Figure 2. It should be noted that both pulses in Figure 2 are adjusted to have the same area under the curves; i.e., the energy contained in these pulses is the same, even though the peak amplitude of the pulse in Case (1) is twice that in Case (2).

1. Case 1. Rectangular Pulse

The surface temperature of the cathode is easily found from Equation (24) for $0 < t < t_o$:

$$T(o,t) = \frac{P_o}{aK} \left(4\frac{\sqrt{\beta t}}{\sqrt{\pi}} - 1 + e^{\beta t} \operatorname{Erfc} \sqrt{\beta t} \right) . \qquad (27)$$

After the laser pulse has stopped, i.e., at $t > t_o$, the general form of the surface temperature is given by

$$T(o,t) = \frac{\beta}{aK} \int_{t-t_o}^{t} P_{to}(t-x)\, g(o,x)\, dx \quad , \qquad (28)$$

or it is simply Equation (27) evaluated at t minus Equation (27) evaluated at $t - t_o$;

therefore for $t > t_o$, we have

$$T(o,t) = \frac{P_o}{aK}\left(4\frac{\sqrt{\beta t}}{\sqrt{\pi}}\left(1 - \sqrt{1 - \frac{t_o}{t}}\right) + e^{\beta t}\ \mathrm{Erfc}\sqrt{\beta t} - e^{\beta(t-t_o)}\ \mathrm{Erfc}\ \sqrt{\beta(t-t_o)}\right). \tag{29}$$

2. Case 2. Sin^2 Pulse

The surface temperature for this case is most easily calculated by writing the light pulse in the following form,

$$P_{to}(t) = P_o - P_o\ \mathrm{Re}\ (e^{j\omega t}) \quad . \tag{30}$$

For $0 < t < t_o$, the evaluation of the convolution integral yields

$$T(o,t) = \frac{P_o}{aK}\left[4\frac{\sqrt{\beta t}}{\sqrt{\pi}} - 1 + e^{\beta t}\ \mathrm{Erfc}\ \sqrt{\beta t}\right] - \left(\frac{\beta^2}{\beta^2+\omega^2}\right)\frac{P_o}{aK}\left[e^{\beta t}\ \mathrm{Erfc}\sqrt{\beta t} - \cos(\omega t)\,A + \sin(\omega t)\,B\right], \tag{31}$$

where

$$A = 1 - 2\sqrt{\frac{2\beta}{\omega}}\ C(\omega t) - \sqrt{\frac{2\omega}{\beta}}\ S(\omega t) \quad , \tag{32}$$

$$B = \frac{\omega}{\beta} - \sqrt{\frac{2\omega}{\beta}}\ C(\omega t) + 2\sqrt{\frac{2\beta}{\omega}}\ S(\omega t) \quad , \tag{33}$$

and the functions $C(\omega t)$ and $S(\omega t)$ are the real and imaginary parts of the Fresnel integral,

$$\frac{1}{\sqrt{2\pi}} \int_0^x e^{-ju} \frac{du}{\sqrt{u}} = C(x) - j\, S(x) \quad . \tag{34}$$

Since surface temperature for $t > t_o$ is simple conceptually, but is rather complex to express, it is not included here. One may find this directly from the result in Equation (31), however, by evaluating it at t and subtracting Equation (31) evaluated at $(t-t_o)$.

Finally, the internal temperature of the cathode may be calculated for these same cases. That for the $\sin^2$ case is very complex; and since only a qualitative description is sought, the results for the rectangular pulse are included here. From Equations (24) and (25), this temperature distribution is found to be

$$T(z,t) = \frac{4P_o}{\alpha K}\left[\frac{\sqrt{\beta t}}{\sqrt{\pi}}\, e^{-\frac{(\alpha z)^2}{4\beta t}} - \frac{\alpha z}{2}\,\mathrm{Erfc}\left(\frac{\alpha z}{2\sqrt{\beta t}}\right) - \frac{1}{4} + \frac{e^{-\alpha z+\beta t}}{4}\right] + \frac{P_o}{2\alpha K}\left[e^{\alpha z+\beta t}\,\mathrm{Erfc}\left(\frac{\alpha z}{2\sqrt{\beta t}} + \sqrt{\beta t}\right) - e^{-\alpha z+\beta t}\,\mathrm{Erfc}\left(\frac{\alpha z}{2\sqrt{\beta t}} - \sqrt{\beta t}\right)\right] . \tag{35}$$

In the limit as $z \to 0$, this expression is seen to yield Equation (27).

D. NUMERICAL EVALUATION OF THE CATHODE TEMPERATURE

It is of interest to evaluate the temperature for a tungsten cathode as a function of time and to estimate the thermionic emission obtained under the conditions for which the maximum thermionic emission was obtained experimentally. The parameters used for tungsten are as follows:

$K = 0.476 \ \frac{cal}{cm \ sec \ °C}$ for thermal conductivity,

$\rho = 19.3 \ \frac{gm}{cm^3}$ for density,

$c_v = 0.034 \ \frac{cal}{g \ °C}$ for heat capacity, and

$2 \ 10^4 \ \frac{mho}{cm}$ = electrical conductivity.

An estimate of the average power density of the laser beam on the cathode surface during a laser pulse or spike can be obtained from a typical laser burst as shown in Figure 11. For a burst lasting 300 μs, there is approximately one spike every 2 μs, and the spike duration at the base line is approximately 0.5 μs. Then, with an energy input to the flash lamp of 500 joules, a threshold of 300 joules, and a laser efficiency of 1 per cent (determined by a separate calorimetric measurement), the total output energy of the laser is approximately 2 joules. The fraction of this energy incident on the tungsten cathode is approximately 0.26, since

the laser output is reduced by one-half by the shutter, and there are at least eight glass-air interfaces from four lenses present (see description of the equipment in Chapter III). The total energy absorbed by the tungsten is determined from the relations in Equations (8) - (11). We have approximately 0.050 joules absorbed by the tungsten during one laser burst. The average absorbed energy for one laser spike is then 3.6×10^{-4} joules. With the conservative estimate of a 0.003-inch diameter spot illuminated on the cathode and the duration of the laser spike estimated previously, the power density at the surface of the cathode is

$$P_o = 3.88\ 10^6 \ \frac{\text{cal}}{\text{sec cm}^2} = 1.62 \times 10^7 \ \text{watts/cm}^2 \quad . \qquad (36)$$

Finally, the parameters α and β are found to be

$$\alpha = 2k\,a = 1.16\ 10^6\ \text{cm}^{-1}, \qquad (37)$$

and

$$\beta = a\ \alpha^2 = 9.75\ 10^{11}\ \text{sec}^{-1} \quad . \qquad (38)$$

For times measured in microseconds, the expressions for the surface temperature of the tungsten as a function of time are simple to approximate because of the values of the parameters just calculated. For the rectangular laser pulse, Equation (27) becomes

$$T(o,t) \simeq \frac{P_o}{aK} \; 4 \frac{\sqrt{\beta t}}{\sqrt{\pi}} \quad . \tag{39}$$

For the $\sin^2$ pulse, the frequency as determined by the estimate of 0.5 μs, base line of pulse is

$$f = \frac{\omega}{2\pi} = 2\ 10^6 \quad ;$$

thus,

$$\frac{\beta}{\omega} = 7.76\ 10^4 \gg 1. \tag{40}$$

Consequently, Equation (31) can be approximated as

$$T(o,t) \simeq \frac{P_o}{aK} \left\{ 4 \frac{\sqrt{\beta t}}{\sqrt{\pi}} - 2\sqrt{\frac{2\beta}{\omega}} \left[C(\omega t \cos \omega t + S(\omega t) \sin \omega t \right] \right\} \tag{41}$$

Plots of the surface temperature as a function of time are shown in Figures 3 and 4 for one laser spike for the two cases considered here. Superimposed on these plots are the assumed shape of the laser spike and the relative electron emissions that would occur thermionically. This emission estimate is obtained by extending the Richardson-Dushman equation to these calculated temperature levels. This technique certainly gives a poor estimate of the emission magnitudes expected, since the calculated temperature is well above the melting point of tungsten, but it gives a reasonable first estimate of the variation of this emission as a function of time. A linear scale is used to represent the calculated current, since this is how the current was viewed experimentally. A

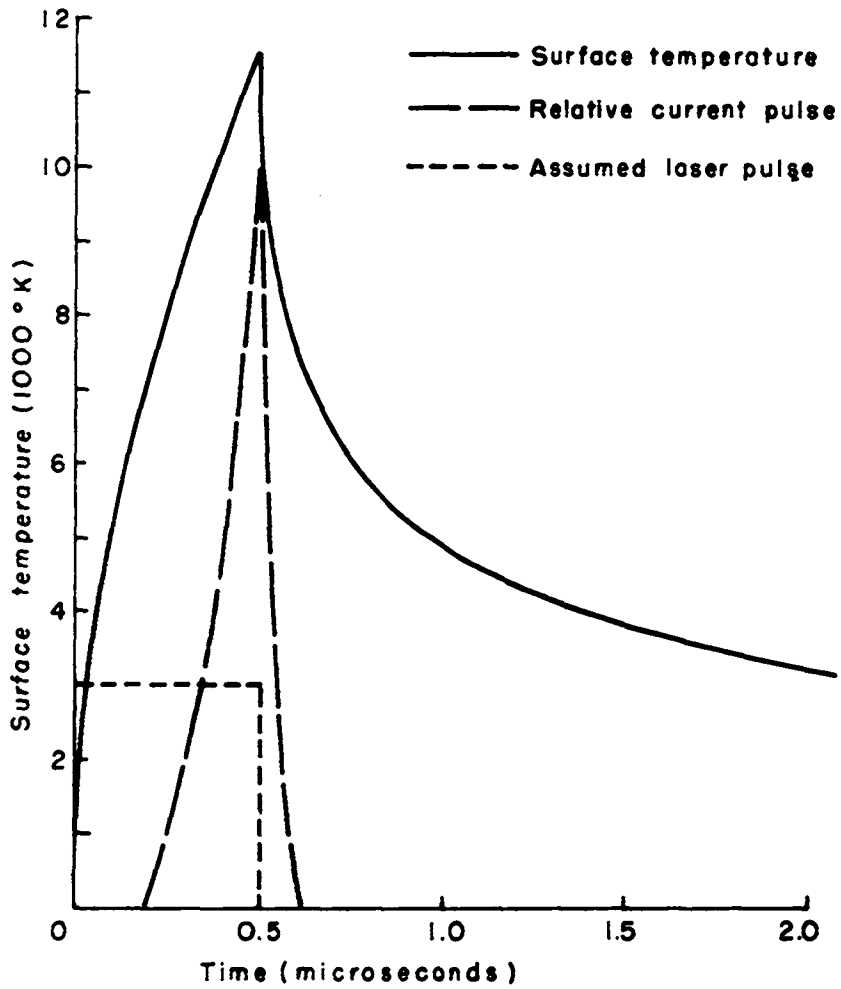

FIGURE 3. Calculated Surface Temperature of Tungsten for Rectangular Laser Pulse.

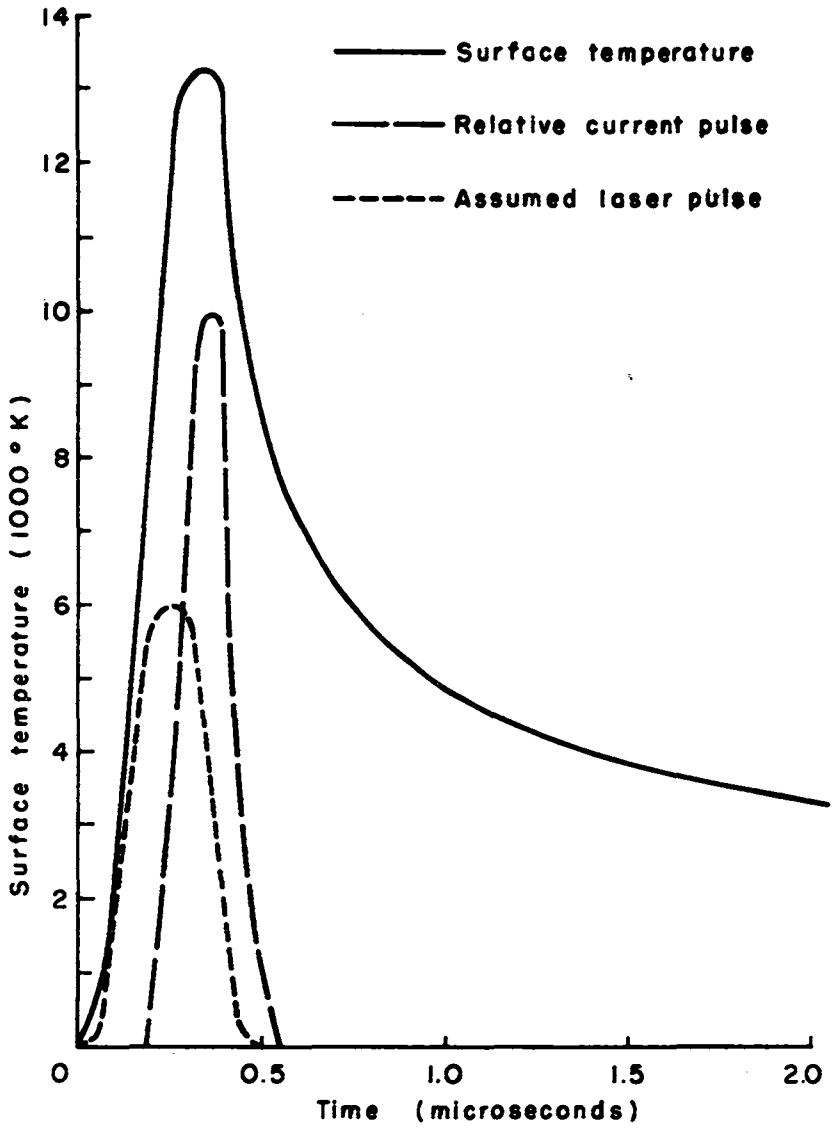

FIGURE 4. Calculated Surface Temperature of Tungsten for Sin^2 Laser Pulse.

discussion of the possibility of having an instantaneous surface temperature greater than the melting point is discussed in Chapter III, where the experimental results are described.

A plot of the interior temperature as a function of the distance from the heated surface is shown in Figure 5. This is the calculated temperature distribution for a rectangular laser pulse at the time when the surface reaches its peak temperature. It should be observed that, although the characteristic penetration distance is small in terms of laboratory dimensions, it is significantly larger than the "skin" depth of approximately 100 A°. This occurs because of the diffusion (in classical terms) of heat energy from the surface.

On the basis of Figure 5, it may be expected that a cathode of finite length would not have a significantly different surface temperature, if the length were greater that 20 μ. An examination of the finite cathode case follows.

E. SURFACE TEMPERATURE OF FINITE CATHODE

A minor difficulty with the semi-infinite cathode model is the failure of the temperature to converge as the time approaches infinity when the laser pulse operates continuously. This is readily evident from Equations (27) and (31). This is not serious in itself, however, since the laser pulse (or series of laser pulses) lasts only for a very short time. The expressions for the temperature after the laser pulse, i.e., $t > t_o$, converge to zero (or room temperature), as the time

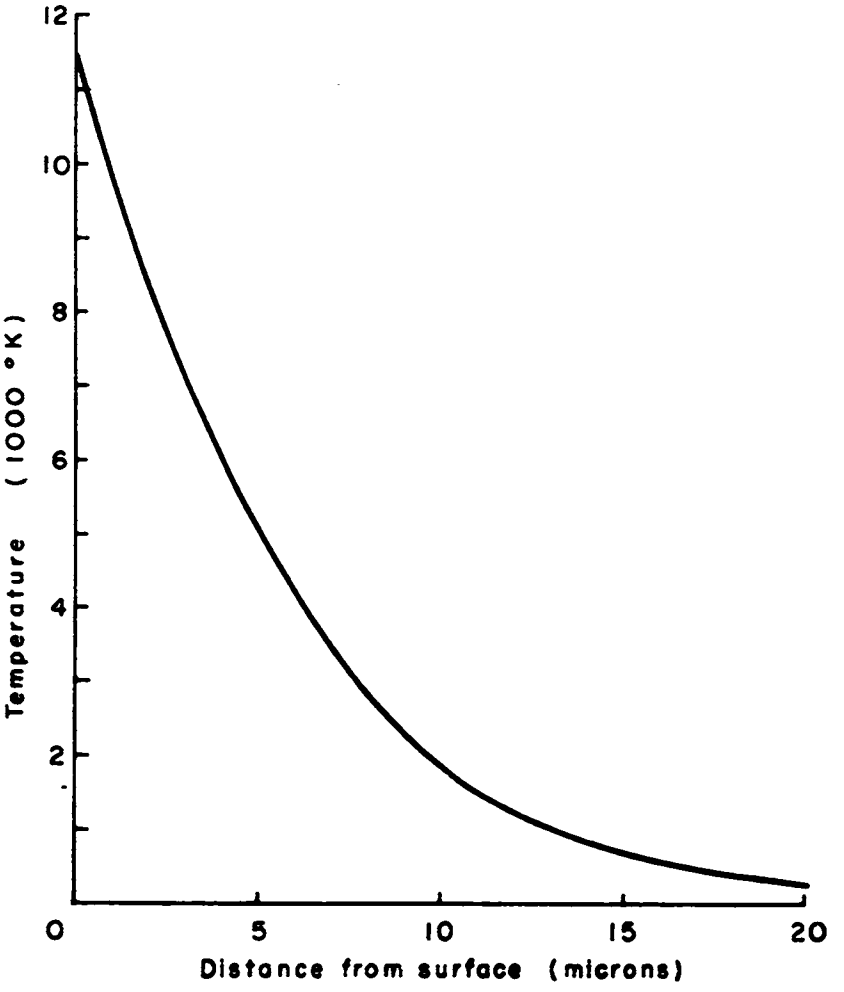

FIGURE 5. Calculated Interior Temperature of Tungsten for Rectangular Laser Pulse at t = 0.5 ms.

becomes very long. The question arises as to how much a finite cathode depth affects the temperature at the surface. This can be answered by considering a cathode model that is infinite in the transverse direction but is finitely long in the z direction (see Figure 1). Consider a cathode that is l meters long in the z direction. The new boundary conditions at the cathode end are chosen by considering the end clamped to a heat sink, i.e.,

$$T(l, t) = 0 \quad ; \tag{42}$$

then Equation (21) still applies, and the solution for $\tau(z, p)$ has the form,

$$\tau(z, p) = Ce^{-\sqrt{\frac{p}{a}}\, z} + De^{\sqrt{\frac{p}{a}}\, z} + \frac{\beta F(p)\, e^{-\alpha z}}{\alpha K(p - \beta)} \quad . \tag{43}$$

The coefficients C and D are found by utilizing the boundary conditions and initial conditions in Equations (17), (19), and (42), which give

$$D = -\frac{F(p)}{\left(1 + e^{2\sqrt{\frac{p}{a}}\, l}\right)} \left[\frac{\sqrt{\beta}}{\alpha K\sqrt{p}} + \frac{\beta^{3/2}}{\alpha K\sqrt{p}(\beta - p)} + \frac{\beta}{\alpha K} \frac{e^{-\alpha l + \sqrt{\frac{p}{a}}\, l}}{(p - \beta)} \right], \tag{44}$$

$$C = \frac{\beta F(p)}{\alpha K(\beta - p)} e^{-\alpha l + \sqrt{\frac{p}{a}}\, l} + e^{2\sqrt{\frac{p}{a}}\, l} D \quad . \tag{45}$$

The surface temperature can be found from the convolution integral in Equation (24). In doing this, the simplest way to evaluate $g(o, t)$ is to

expand the exponential functions in Equations (43), (44), and (45) in the following way:

$$\frac{e^{2\sqrt{\frac{p}{a}}l} - 1}{e^{2\sqrt{\frac{p}{a}}l} + 1} = 1 + 2 \sum_{n=1}^{\infty} (-1)^n e^{-2nl\sqrt{\frac{p}{a}}} \quad . \tag{46}$$

The result found for the surface temperature for a rectangular laser pulse and for $0 < t < t_o$ is

$$T(o,t) =$$

$$\frac{P_o}{aK}\left[\frac{4\sqrt{\beta t}}{\sqrt{\pi}} - 1 + e^{\beta t}\ \mathrm{Erfc}\ \sqrt{\beta t}\right]$$

$$+ \frac{P_o}{aK}\ e^{\beta t} \sum_{n=1}^{\infty} (-1)^n \left[e^{2nal}\ \mathrm{Erfc}\left(\frac{nal}{\sqrt{\beta t}} + \sqrt{\beta t}\right) - e^{-2nal}\ \mathrm{Erfc}\left(\frac{nal}{\sqrt{\beta t}} - \sqrt{\beta t}\right)\right]$$

$$- \frac{P_o}{aK}\ e^{-al+\beta t} \sum_{n=0}^{\infty} (-1)^n \left[e^{2al(n+1/2)}\ \mathrm{Erfc}\left(\frac{al(n+1/2)}{\sqrt{\beta t}} + \beta t\right)\right.$$

$$\left. + e^{-2al(n+1/2)}\ \mathrm{Erfc}\left(\frac{al(n+1/2)}{\sqrt{\beta t}} - \sqrt{\beta t}\right)\right]$$

$$+ \frac{2\,P_o}{aK}\ e^{-al} \sum_{n=0}^{\infty} (-1)^n\ \mathrm{Erfc}\left(\frac{al(n+1/2)}{\sqrt{\beta t}}\right) \quad . \tag{47}$$

The most useful result obtained from this expression for the surface temperature of the finite cathode is that the series are negligible, provided

$$\alpha l \gg \sqrt{\beta t} \quad . \tag{48}$$

If this condition is satisfied, then Equation (47) reduces to Equation (27), the surface temperature for the infinite cathode. For the time scales involved in Section D, the condition on the cathode length becomes approximately

$$l \gg \frac{10^{-3}}{10^{6}} = 10^{-3} \text{ cm} \quad , \tag{49}$$

a condition which is readily met in practice and which was suggested by the results shown in Figure 5.

For the finite material, it is of interest to examine the long-term or steady-state surface temperature for a continuous and periodic excitation, because this is a convenient means of seeing how well the surface temperature can follow periodic fluctuations in the intensity of the incident laser beam. The transient solution for the temperature for a periodic input can be obtained from Equation (31), but this will not converge as the time becomes infinite, because an infinite cathode model is assumed. If a finite model is used, however, then a steady-state temperature can be found. It might be observed that this result is not restricted to the temperature calculation here, but is characteristic of any diffusion equation for a one-dimensional, infinite model.

We now consider the case where the surface temperature of the finite cathode for a continuous input is of the form given in Equation (30). Since the form of Equation (16) is linear, we can solve separately for the d-c and a-c parts of Equation (30) and add the resultant solutions. The solution for the surface temperature for the d-c part of the input is contained in Equation (47), but unfortunately it cannot be used directly. Equation (47) is valid for all finite values of time; but if we take the limit as time becomes infinite, this expression does not converge, because the series in Equation (46) used in the Fourier transform of the kernel $g(o, t)$ is not valid for $p = 0$. The simplest way to obtain the desired solution, therefore, is to return to the original differential equation and solve directly for the steady-state solutions.

The steady-state d-c solution is obtained from the following form of Equation (16),

$$\frac{\partial^2 T(z)}{\partial z^2} = - \frac{a}{K} P_o \; e^{-az} \quad . \tag{50}$$

The general solution of this differential equation is

$$T(z) = - \frac{P_o}{aK} \; e^{-az} + C_1 z + C_2 \quad ; \tag{51}$$

then the boundary conditions in Equations (19) and (42) can then be used to determine the constants of integration C_1 and C_2 :

$$T(z) = \frac{P_o}{aK} \left[2a \; (l - z) - e^{-az} + e^{-al} \right] \quad ; \tag{52}$$

and the surface temperature is found to be

$$T(0) = \frac{P_o}{aK} \quad (2\,a\,l - 1 + e^{al}) \quad . \tag{53}$$

It is observed that as l becomes infinitely large, the surface temperature also becomes infinitely large.

The steady-state a-c solution can be found from Equation (16) by assuming a solution with a time variation of $e^{j\omega t}$. Then if we let

$$T(z,t) = \mathrm{Re}\left[e^{j\omega t} \quad V(z)\right] \quad , \tag{54}$$

Equation (16) yields

$$V(z) = C_1 \; e^{-\sqrt{\frac{j\omega}{a}}\, z} + C_2 \; e^{\sqrt{\frac{j\omega}{a}}\; z} + \frac{\beta\, P_o\, e^{-az}}{aK(j\omega-\beta)} \quad . \tag{55}$$

From the boundary conditions in Equations (19) and (42), we find

$$C_2 = \frac{P_o}{\sqrt{\frac{j\omega}{a}}\left(1 + e^{2\sqrt{\frac{j\omega}{a}}\, l}\right)} \left[-\frac{1}{K} + \frac{\beta}{K(\beta - j\omega)} - \sqrt{j\,\frac{\omega}{a}}\; \frac{\beta\, e^{-al + \sqrt{j\frac{\omega}{2}}\, l}}{aK(\beta - j\omega)}\right], \tag{56}$$

$$C_1 = \frac{\beta\, P_o\, e^{-al\, +\, \sqrt{j\frac{\omega}{a}}\, l}}{aK\,(j\omega - \beta)} - C_2\, e^{2\,\sqrt{j\,\frac{\omega}{a}}\, l} \quad . \tag{57}$$

For simplicity, let

$$u = \alpha l \sqrt{\frac{\omega}{2\beta}} \quad ; \tag{58}$$

then one finds,

$$V(o) = \frac{P_o}{aK} \frac{1}{(1 - j\frac{\omega}{\beta})} \left[-1 + \left(\frac{1 - e^{2u\sqrt{2j}}}{1 + e^{2u\sqrt{2j}}} \right) \left(\sqrt{j\frac{\omega}{\beta}} - \frac{2}{\sqrt{j\frac{\omega}{\beta}}} \right) + \frac{2\, e^{-\alpha l + u\sqrt{2j}}}{1 + e^{2u\sqrt{2j}}} \right] \tag{59}$$

A considerable simplification of this expression results if the conditions,

$$\alpha l \gg 1, \quad \sqrt{\frac{\omega}{\beta}} \ll 1 \quad , \tag{60}$$

are used. From Section D, these conditions are seen to be easily satisfied in a practical case. With these restrictions we find

$$V(o) \simeq \frac{P_o}{aK} \left[\frac{2}{\sqrt{j\frac{\omega}{\beta}}} \tanh\left(u\sqrt{2j}\right) - 1 \right] \quad ; \tag{61}$$

consequently, the surface temperature is found to be

$$T(z,t) = | V(o) | \cos(\omega t + \phi) \quad , \tag{62}$$

where

$$| V(o) | = \frac{P_o}{aK} \left[2(b^2 + d^2) - 2(b + d) + 1 \right]^{1/2} \tag{63}$$

$$\tan \phi = -\left(\frac{b - d}{b + d - 1}\right) \quad , \tag{64}$$

and

$$b = \sqrt{\frac{2\beta}{\omega}} \left[\frac{\sinh (2u)}{\cosh (2u) + \cos (2u)} \right] , \tag{65}$$

$$d = \sqrt{\frac{2\beta}{\omega}} \left[\frac{\sin (2u)}{\cosh (2u) + \cos (2u)} \right] . \tag{66}$$

Finally, the steady-state solution for the surface temperature when the laser beam is continuously described by Equation (30) is

$$T(z, t) = \frac{P_o}{aK} \left(2al - 1 + e^{-al}\right) - | V(o) | \cos (\omega t + \phi) \quad . \tag{67}$$

A sketch of the ratio of the a-c to d-c surface temperature of a tungsten cathode is shown in Figure 6 as a function of the cathode depth l . This figure is of doubtful value for distances shorter than a few microns, since the boundary condition at $z = l$ in Equation (42) is no longer realistic physically. For longer distances, the ratio in Figure 6 is inversely proportional to cathode length, because the average temperature is directly proportional to cathode length, whereas the fluctuating component of the temperature is nearly constant. The phase angle ϕ in Equation (64) gives a delay of zero degrees at small lengths and a maximum delay of 45 degrees at large lengths.

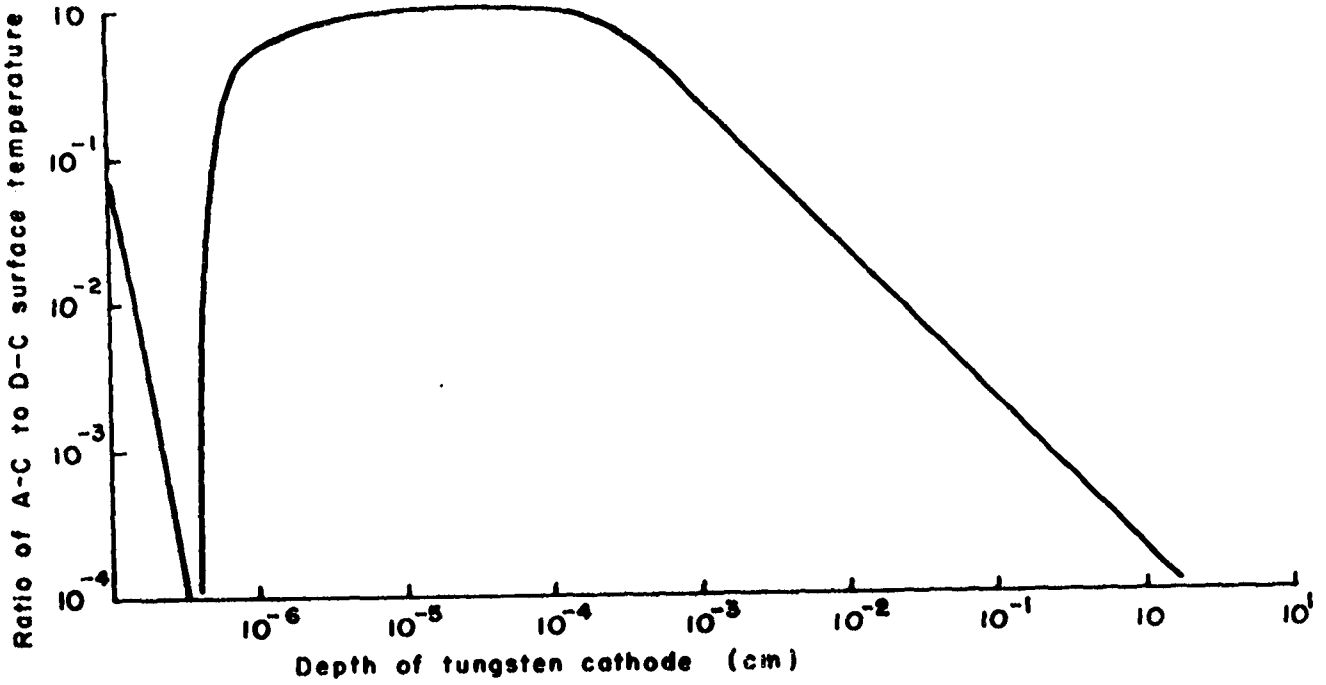

FIGURE 6. Calculated a-c to d-c Surface Temperature Ratio for Tungsten in the Steady-State Case.

Thus for cathode lengths greater than about 10 microns, the a-c component of the surface temperature is relatively constant. For long lengths, the theory shows that this variation in temperature is not very significant because the average temperature is so high. The practical significance of the variation of the a-c component is not clear for several reasons. First, the average steady-state temperature predicted by this theory for cathode lengths greater than 10 microns is so high that the linearized heat equation is no longer valid. Also, the time required to reach this steady-state d-c temperature is long, compared to the length of one laser pulse. The indication from Equation (41), however, is that the a-c component of the surface temperature reaches its steady-state value very quickly, for $C(\omega t)$ and $S(\omega t)$ are nearly constant for $t \geq 0.5$ μs. It would be expected then that the ratio plotted in Figure 6 would be larger in the transient state before the d-c temperature has reached its final value under a continuous laser-beam input. Perhaps the most significant information obtained from the calculations in this section is that the surface temperature in the linearized one-dimensional classical model will follow the assumed 2-megacycle variation in the laser beam intensity. The ratio $\sqrt{\beta/\omega}$ will have to become smaller by one order of magnitude before the surface temperature no longer follows the variations in the laser beam. This would require a frequency of approximately 200 Mc/s.

F. ESTIMATE OF RADIATION LOSS

The loss of energy from the cathode surface by radiation was neglected in Sections B through Section E. Since this loss varies as the fourth power of the surface temperature, it could have an important effect for the high surface temperatures calculated here. Its importance can be estimated by examining the boundary conditions at $z = 0$ when this loss is accounted for. Instead of Equation (18), the complete boundary condition should be

$$\frac{\partial T}{\partial z}\ (o,t) = -\frac{1}{K}\ P_{to}\ (t) + \frac{\epsilon \mu}{K}\ T^4(o,t) \quad , \tag{68}$$

if it is assumed that radiation is occurring into a medium at absolute zero temperature. The parameter ϵ is the emissivity (about 0.4 for tungsten at a wavelength of 6000 A°), and μ is given by

$$\mu = 5.67\ 10^{-5}\ \frac{\text{erg}}{\text{cm}^2\ \text{sec deg}^4} \quad . \tag{69}$$

During the laser pulse, however, this correction is relatively unimportant, as may be seen by using the numbers in Section E for the rectangular laser pulse, which gives

$$\left.\frac{\frac{\epsilon \mu}{K}\ T^4(o,t)}{\frac{1}{K}\ P_{to}(t)}\right|_{t = 0.5\ \mu s} = 2.5\ 10^{-3} \quad . \tag{70}$$

Consequently, the loss of energy from the cathode by radiation does not significantly decrease the calculated peak temperature; but after the laser pulse has ceased, this energy loss will be important, because the term in Equation (68) that depends on $P_{to}(t)$ is zero for $t > 0.5$ μs. The conclusion is that the radiation loss will not affect the rise time or the peak value of the surface temperature, but will force a more rapid cooling of the surface than is indicated in Figures 3 and 4.

The surface temperature can be calculated to include radiation loss by utilizing the nonlinear boundary condition in Equation (68) and assuming a series expansion for the surface temperature. Then a term-by-term solution may be obtained from the heat equation for the coefficients of the assumed expansion. Unfortunately, the convergence of the series is so slow for times on the order of a few tenths of a microsecond or longer that this solution is impractical, and will not be included here.

G. SUMMARY AND EVALUATION OF THEORETICAL CALCULATIONS

The theory presented in this section has utilized the linearized, classical heat-flow equation applied to a one-dimensional model. A classical field description has been given for the incident light beam to calculate the portion of the incident energy absorbed and the rate, with distance, at which this has been absorbed in the cathode material. A crude estimate of the electron emission has been based only on the calculated rise in surface temperature following the semiclassical theory of thermionic emission of the Richardson-Dushman equation.

The principal results of this theory are that the surface temperature has a very fast rise time and that it reaches a high peak value, which is maintained for a very short time interval. The relative electron-emission current on a linear scale consists of a narrow spike slightly delayed with respect to the light pulse. Finally, this simple theory indicates that the surface temperature can follow rapid time variations in the incident light intensity at frequencies as high as several mega-cycles per second.

There are several omissions in the theory presented here, some of which are serious. If one wishes to pursue the classical calculation of the surface temperature, the most serious assumption is that of linearity. The temperature change is so large that parameters such as the heat capacity and electrical conductivity change appreciably. Accounting for these changes would result in Equation (12) being a non-linear differential equation. Also, of course, the inclusion of the energy radiation loss in describing the cooling of the surface after the light pulse has ceased results in a nonlinear boundary condition. Once these corrections are included, one should examine the characteristic of the resultant temperature versus time and decide if some accounting should be made for material lost from the surface by vaporization during the peaks of the temperature cycles. There is experimental evidence that this does occur for the higher laser energies used to obtain thermionic emission of electrons. It is possible that a classical accounting of any material lost may be made by utilizing a "shock"-wave or "blast"-wave theory. Any loss of material from the cathode surface during a laser pulse will act to cool the surface and will affect the emission of electrons.

So far, this describes the failings of the present theory in determining the temperature of the cathode material. The next concern is its usefulness in the calculation of the expected electron emission. At the least, one could improve the present estimate by performing a time-dependent calculation, depending on the distribution of electron energies in the vicinity of the surface of the cathode material. Because of the high electron energies, some electrons will take part in the thermionic emission, but there is also a flow of electrons away from the surface that contributes to the diffusion of heat energy away from the surface. This effect will tend to reduce the thermionic emission one would calculate otherwise and is one of the reasons that only a relative emission current density was shown in Figures 3 and 4.

It has been mentioned several times that a theory based on quantum mechanics should be developed to describe the heating of the cathode material by the laser beam and the resultant electron emission adequately. The principal reason for this is that the wavelength of the incident radiation is shorter than that for infrared radiation, which is usually taken as the rough dividing line between considering radiation of materials by classical or by quantum theory. This is evidenced by the "skin depth" for absorption in the cathode material being approximately 100 A°, which is only a few tens of molecular layers and is therefore comparable to dimensions measured in terms of the crystal lattice. Also, the phenomenon of thermionic emission of electrons is properly calculated from quantum theory, and not from the semi-classical theory represented by the Richardson-Dushman equation. Finally, if the surface reaches a high peak temperature, then the

energy distribution of electrons may be shifted sufficiently above the Fermi level that some direct photo emission of electrons may occur in addition to the thermionic emission. This could occur even though the work function of tungsten is approximately 4.5 ev and the energy of the laser beam is 1.78 ev at 6943 A°. The simple classical theory presented here is just a first approach to explaining the rather complex series of events that occur at and near the surface of a metallic material, when it is illuminated by an intense laser beam.

III. EXPERIMENTAL OBSERVATIONS

An extensive series of experiments were conducted to examine the emission of particles from a target when illuminated by a focused laser beam. The target material (the cathode) was tungsten, except in one case, when a stainless-steel structure was accidentally bombarded before a workable means of directing the laser beam was devised. This chapter describes the arrangement and operation of equipment, shows a sample of some of the data obtained, and discusses the observations made.

A. DESCRIPTION OF EQUIPMENT

All the experiments described here used a pulsed laser with a ruby crystal which operated at a wavelength of 6943 A°. The ruby crystal, 1/4-in. in diameter by 6 in. long, was aluminum oxide with 0.05 per cent chrominum doping, and the optic axis had a 90° orientation. The transmitting end was flat and uncoated, while the reflecting end had a two-facet chisel point. The crystal and a linear flash tube, an EGG type FX-45, were contained in an elliptical housing which had polished stainless-steel reflectors coated with silicon monoxide. An exploded view[1] of the laser housing is shown in Figure 7.

The power supply for the laser consisted of a conventional d-c power supply, which charged a capacitor bank to a predetermined voltage, and a triggering circuit to provide a pulse of approximately 15 kv to the triggering wire on the flash tube. The capacitor bank, which

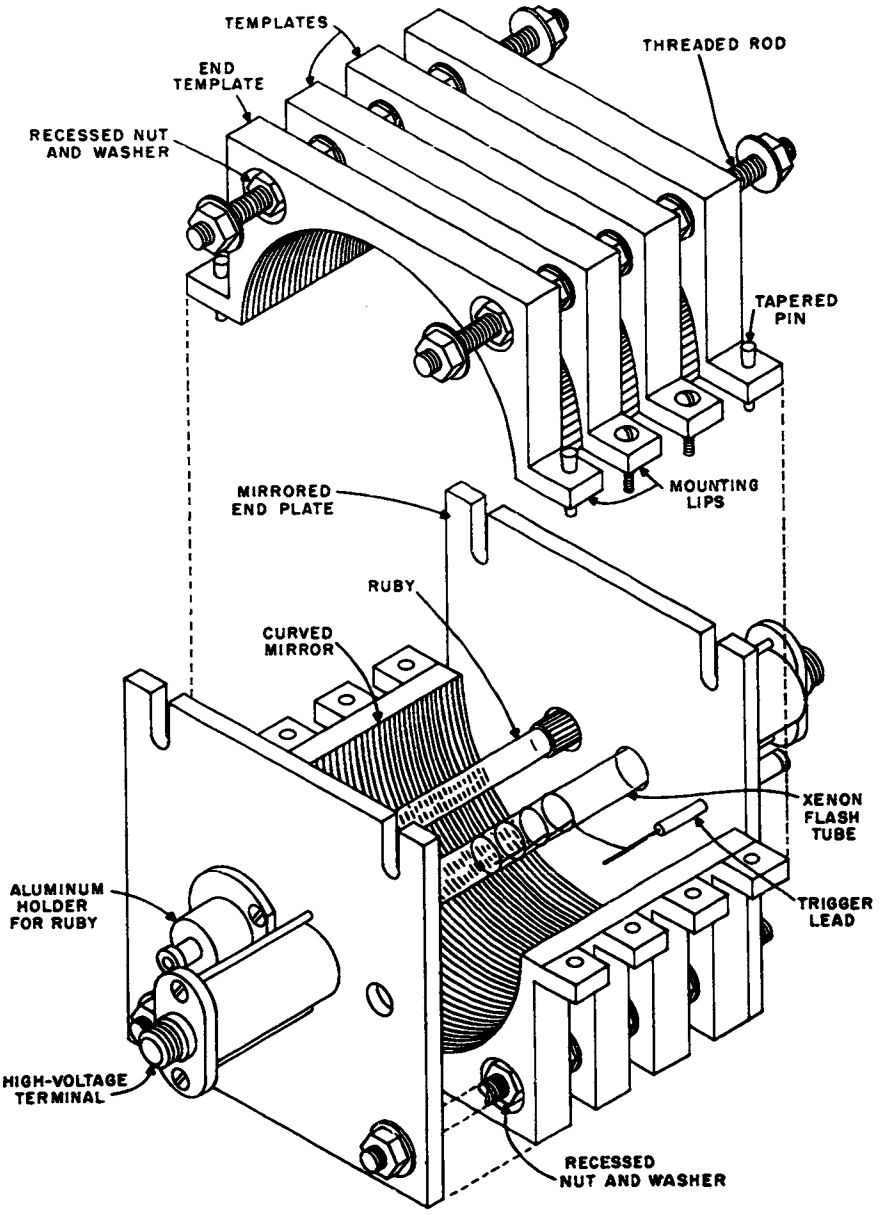

FIGURE 7. Exploded View of Laser Housing.

could be 120, 240, or 600 μf, had an energy-storage capability of 2700 joules. The threshold energy for the laser was approximately 300 joules, and the efficiency, as determined by a separate calorimetric measurement of the output energy, was slightly greater than 1 per cent.

All of the emission tests described here were conducted with the same vacuum structure, but different cathodes and particle-collecting structures were inserted inside. Two different configurations were used for the experiments. The first was a cylindrical copper anode, approximately 2 in. long and 3/4 in. in diameter. The cathode was a tungsten wire aligned with the axis of the cylindrical anode and partially inserted inside the anode. Several different cathodes were used in this geometry. The second configuration used two parallel-plane anodes, which were electrically isolated. Attached to each of these anodes was a coarse gride, which was electrically isolated from the anode. The only cathode used in this configuration was a ten-mil tungsten wire placed in a plane parallel to the anodes. In this configuration the laser beam illuminated a spot on the side of the tungsten wire, whereas in the first configuration the laser beam was focused on the end of the wire. Figure 8 shows the vacuum structure with the first configuration in place (called the first diode structure hereafter), and Figure 9 shows details of the second configuration (called the second diode structure hereafter).

The vacuum shell, which was made of stainless steel, was evacuated by an ion pump. The operating pressure with the first diode structure was in the high 10^{-9} Torr range while that with the second diode structure was in the low to middle 10^{-8} range. The vacuum

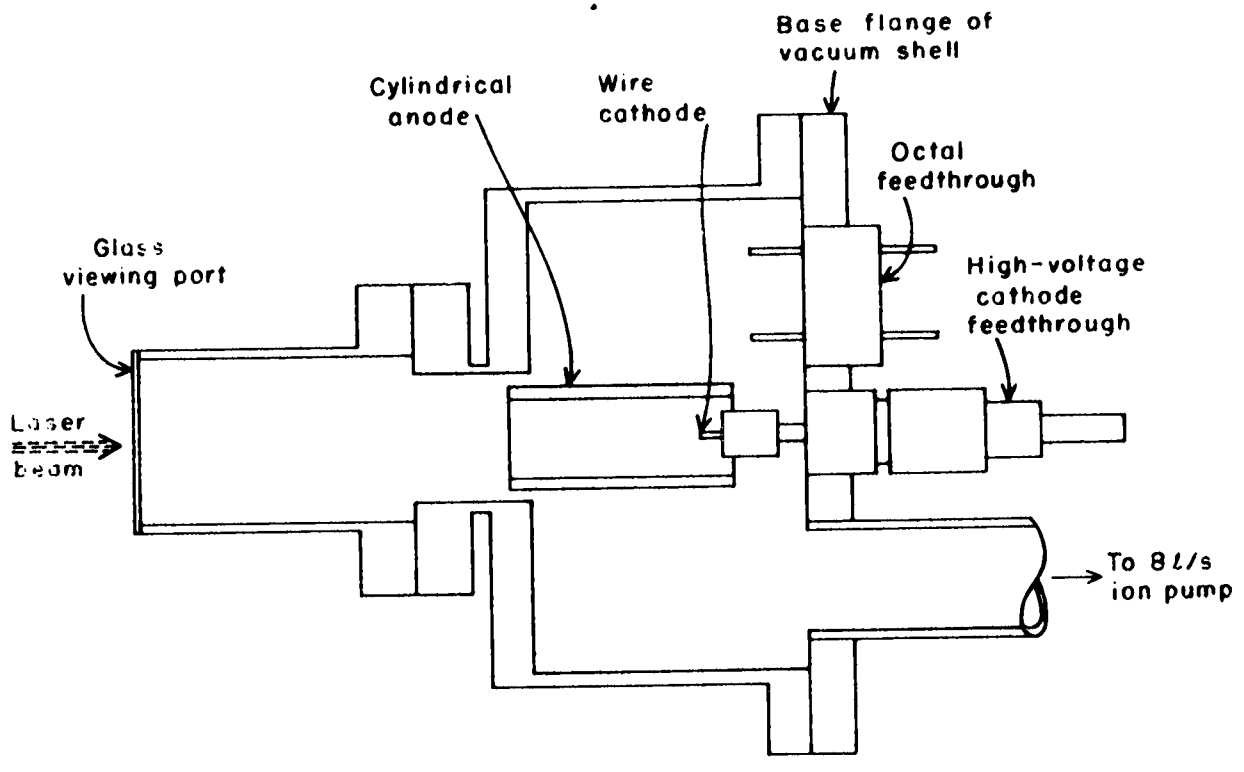

FIGURE 8. Three-Fourths Scale Drawing of Vacuum Shell and First Diode Structure (Anode Is Connected to a Second High-Voltage Feedthrough).

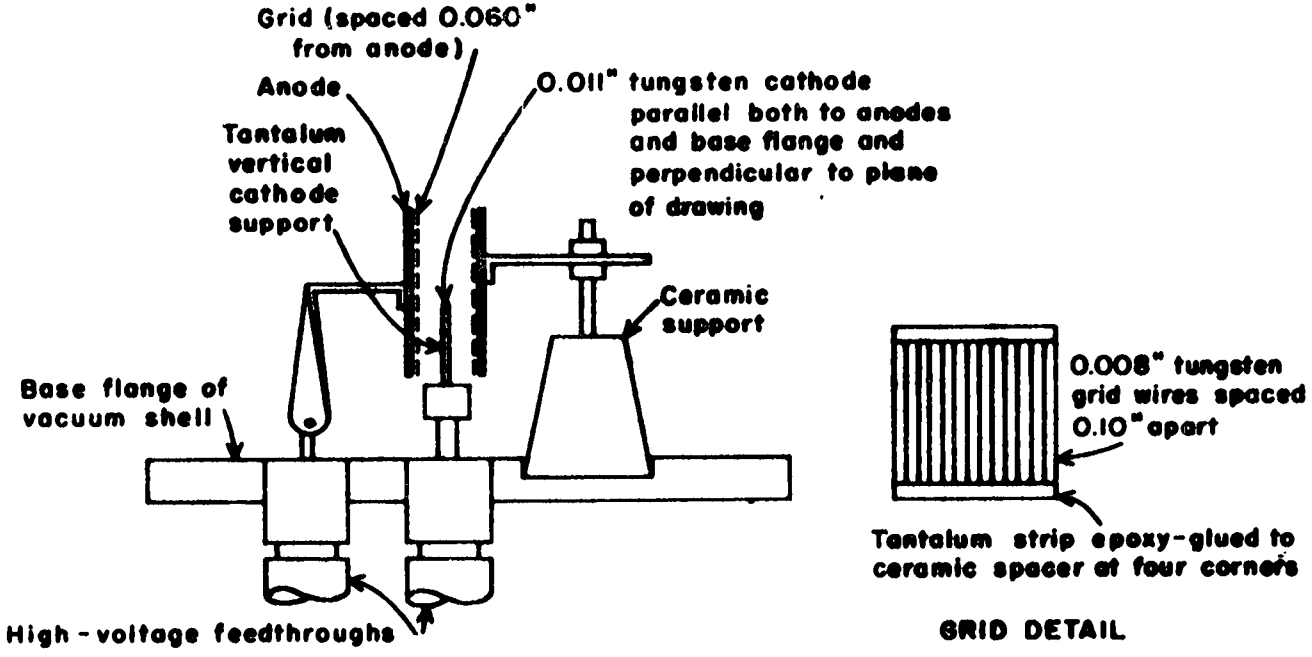

FIGURE 9. Three-Fourths Scale Drawing of Second Diode Structure.

was somewhat worse in the second diode structure because an epoxy glue was used to support the grid structures.

The remaining principal part of the equipment was the optical system for focusing and controlling the laser beam. A telescope of 5.5x power was placed between the laser housing and the test diodes, with the eyepiece closest to the laser. The laser beam was expanded upon traversing the telescope and its angular divergence decreased. A rotary shutter was placed on the objective end of the telescope to provide a smooth control of the laser intensity incident on the cathode. This was used in preference to an iris shutter to avoid defocusing the laser beam at small apertures. Finally a focusing lens with a 7-in. focal length was placed in front of a view port on the vacuum shell of the diode structure. This lens was adjusted to move axially to control the focusing of the laser beam, while the objective end of the telescope was translated horizontally and vertically to control the point of impact of the laser beam. The laser beam was positioned on the target optically by inserting a small mirror in front of the focusing lens and then firing the laser just above threshold. Since the cathode was close to the focal point of the lens, this provided an enlarged view of the cathode. Finally a monocular was used to observe the cathode in the small mirror. With the shutter open a few degrees and suitable attenuators placed in front of the monocular, the laser spot on the cathode was just barely visible. This procedure gave good control of the positioning of the laser beam on the cathode, for it was possible to move the small spot on the end of a 10-mil tungsten wire at will. A block diagram of the complete apparatus is shown in Figure 10.

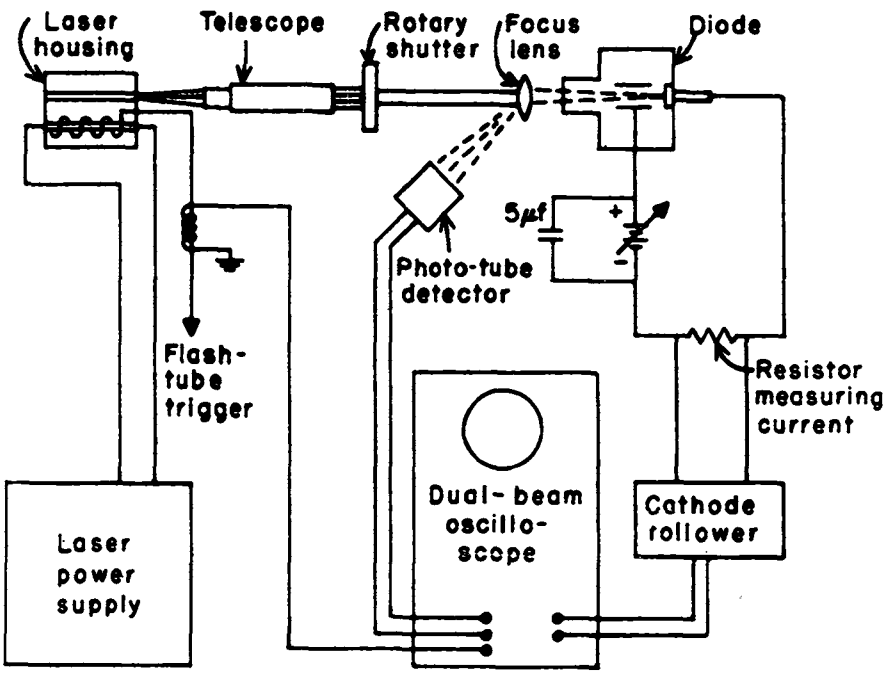

FIGURE 10. Block Diagram–Laser-induced Emission Experiment.

A phototube detector was used to observe the output intensity of the laser as a function of time. This detector, which used an RCA 925 phototube, was located so that it picked up the small amount of reflected light from the front surface of the focusing lens. To help give a good high-frequency response, the phototube was operated at a low current and a small one-stage amplifier was included in a common housing with the phototube. The output of this circuit was usually displayed on one trace of a dual-beam oscilloscope, along with the diode current resulting from the laser burst.

B. EXPERIMENTAL RESULTS

Four distinct types of emission were observed from the various cathodes used, depending upon the operating conditions. These were the thermionic emission of electrons, ion emission, a tungsten plasma discharge with the anode positive with respect to the cathode, and a reverse plasma discharge with the anode negative. Each of these is described in this section and some preliminary data are given for a heated cathode in the second diode structure.

1. Thermionic Emission

Typical data showing the thermionic emission of electrons are shown in Figures 11, 12, and 13. Then data were obtained from the first diode structure with the anode 500 volts positive with respect to the cathode. In all these photographs, the lower trace is the phototube response to the laser light beam; and the upper trace is the diode current,

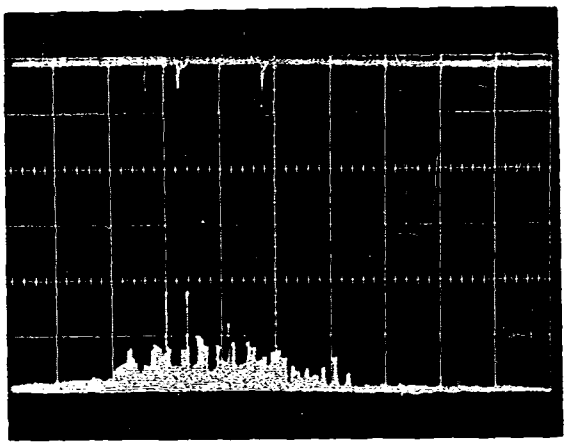

(a)

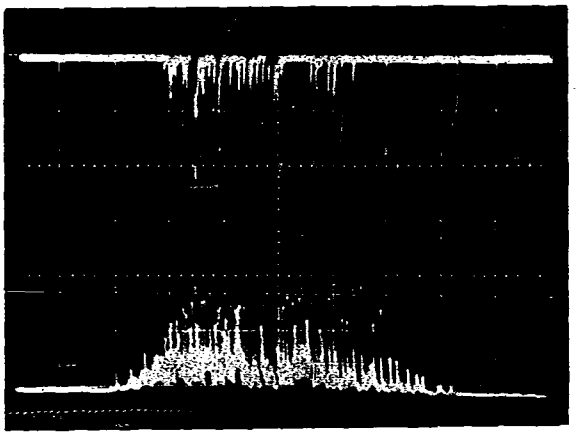

(b)

FIGURE 11. Thermionic Electron Emissions. Anode: 500 v Positive with Respect to Cathode. (a) Current Scale: 1 μa/div., Time Scale: 50 μs/div.; (b) Current Scale: 150 μa/div., Time Scale: 50 μs/div.

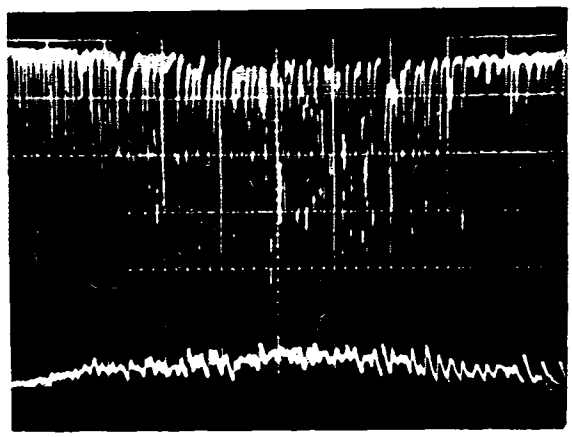

(a)

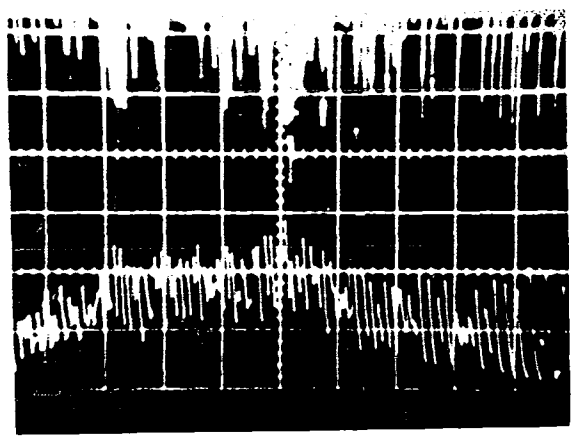

(b)

FIGURE 12. Thermionic Electron Emissions. Anode:500 v Positive with Respect to Cathode. (a) Current Scale: 40 ma/div., Time Scale: 20 μs/div.; (b) Current Scale: 100 ma/div., Time Scale: 20 μs/div.

where a downward deflection is electron current collected at the anode. Note that the phototube frequency response is poor in Figure 12 and Figure 13.? For obtaining the data shown in Figure 11, the response had been improved. These data were taken as a function of increasing output energy of the laser, ranging from 0.13 joules incident on the cathode surface to 0.60 joules. The data shown in these figures were selected from a larger group taken by using both a 20-mil diameter tungsten wire and a 0.190-in. diameter tungsten rod as cathodes. The tungsten rod was a zone-refined single crystal, although a single crystal face was not exposed to the laser beam, because the rod was ground flat and etched at a random location on the axis. The 20-mil tungsten wire was ordinary high-purity wire, which was at first thought to be amorphous. An examination of a polished and etched end of this wire with a Unitron metallographic microscope revealed no grain boundaries, however, so that this material probably had a single crystal surface exposed to the laser beam. Three different 20-mil wires were used, each with a different surface preparation. One wire had a ground end; another had a ground and polished end; and the third had a ground, polished, and etched end. The results of the emission experiments using these three tungsten wires and the tungsten rod were essentially identical; however, small differences in the relationship between the peak emission density and the incident laser energy (which might be expected to arise because of the different reflectivities of the various surfaces) were not sought.

As indicated in Figure 13, the peak emission current is at least 700 ma. Based on a conservative estimate of a 3-mil diameter emission spot, the calculated electron current density is approximately 1.5×10^4

a/cm^2. An upper bound on the emission density for the case in Figure 13 is obtained by choosing 800 ma as the peak current and a one-mil diameter emission spot, on the assumption that the center of the illuminated area is very hot compared to the outer edges. This estimate yields an emission current density of 1.6×10^5 a/cm^2. The emission area was determined by illuminating the cathode face several times with the laser beam at an energy midway between that used for Figures 11, 12, and 13. Under these conditions, the illuminated spot becomes glossy in appearance, as though the surface had momentarily melted and then refrozen. A photomicrograph of the cathode face was made and the spot size measured from this. A sample of a photomicrograph of the cathode face is shown in Figure 14. The ring in figure 14a shows one of the spots slightly damaged by the laser beam. This spot is oval and measures approximately 0.001 in. by 0.003 in.

When the anode voltage was increased for the emission case illustrated in Figures 11 and 12, the diode current remained constant, which indicates that all the emission current was being collected. As the anode voltage was decreased to zero and to slightly negative values with respect to the cathode, interesting results were observed. Figures 15 and 16 show the data for decreasing anode voltage when the laser output energy was approximately that required to obtain a maximum thermionic emission of electrons. In these figures, the lower trace is the phototube output; the upper trace is the diode current, where an upward deflection indicates electron current collected at the anode. At low positive voltages, the spikes in the electron emission shown in

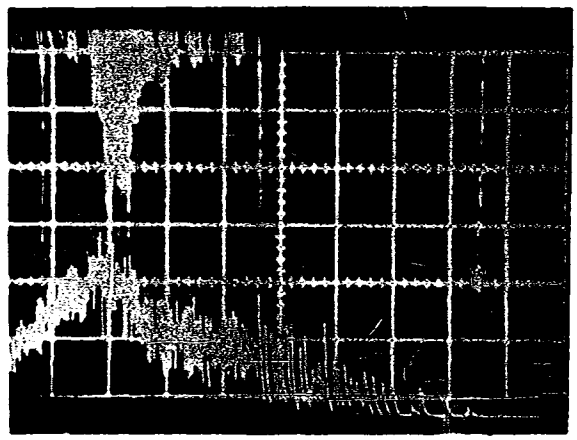

FIGURE 13. High-Density Thermionic Electron Emission. Current Scale: 200 ma/div., Time Scale: 50 μs/div., Anode: 500 v Positive with Respect to Cathode.

Figures 11 and 12 are suppressed in the middle of the laser burst by the space charge present, and a continuous current was observed during the laser burst. The electron current does show spikes near the start of the pulse, where sufficient space charge had not built up to limit the anode current. Apparently an average current during the burst is required to give a heavy space-charge limitation to the occurence of a spike. The fact that a large electron current is collected at the anode for zero applied volts is indicative of a high average electron energy, i.e., it may be a large fraction of an electron volt. This means that the effective surface temperature must be very high, which is emphasized by the suprisingly large electron current shown in Figure 16

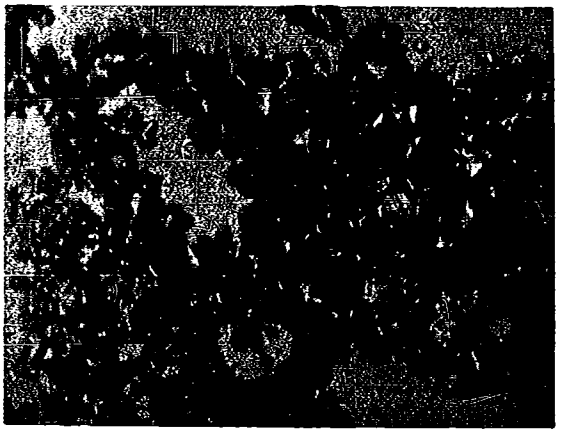

(a)

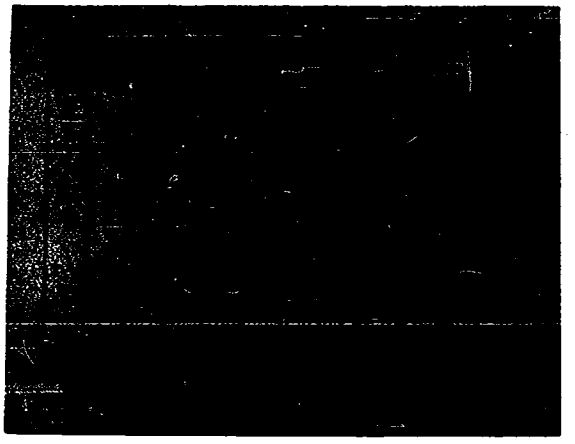

(b)

FIGURE 14. Photomicrograph of 0.190-in. Tungsten Rod. (a) Circled Spot Slightly Damaged by Laser Beam; (b) .001-in. Grid Taken at Same Magnification as (a).

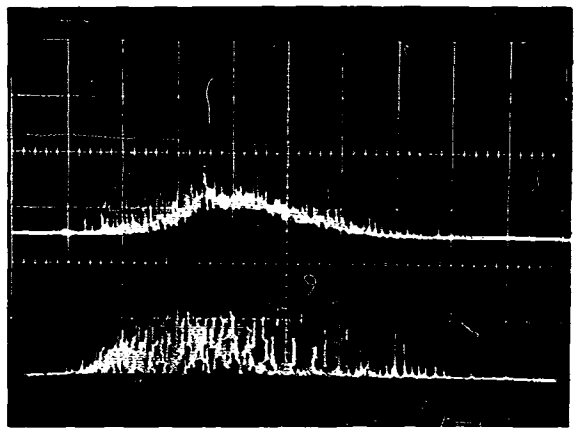

(a)

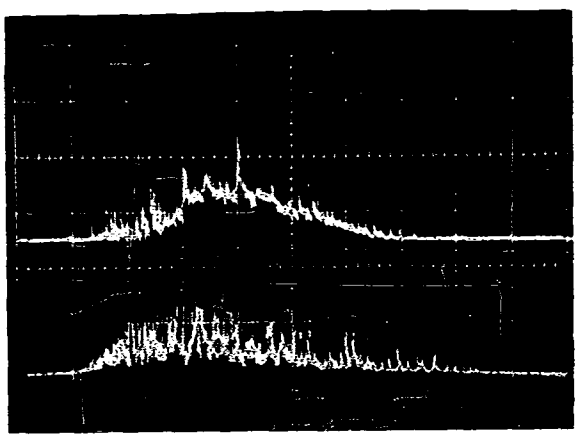

(b)

FIGURE 15. Electron Emission in Retarded Field Region.
(a) Anode: + 20 v, Current Scale: 2 ma/div., Time Scale: 50 μs/div.;
(b) Anode: 0 v, Current Scale: 500 μa/div., Time Scale : 50 μs/div.

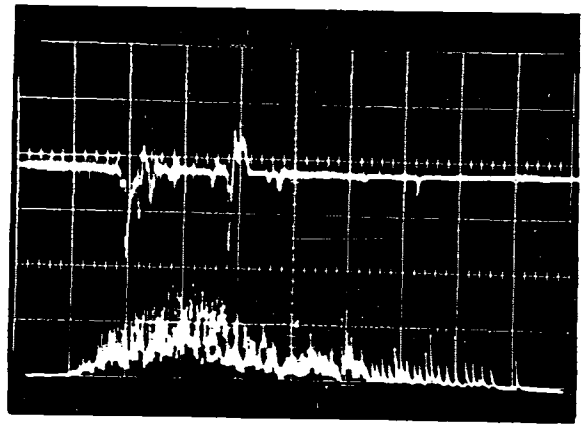

(a)

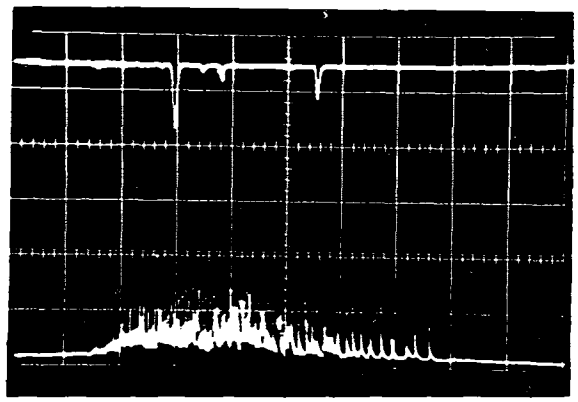

(b)

FIGURE 16. Electron Emission in Retarding-Field Region.
(a) Anode: -6 v, Current Scale: 300 μa/div., Time Scale: 50 μs/div.;
(b) Anode: -75 v, Current Scale: 200 ma/div., Time Scale: 50 μs/div.

for an anode voltage of minus 6 v with respect to the cathode. Here only spiked electron currents are collected at the anode, and the average current during the burst is suppressed. The downward deflection in the current traces are indicative of ion current collected at the anode. The ion current spikes are broader than those for the electron current, which is as expected because of the heavier mass of the ions. For large negative anode voltages, the electron current is completely suppressed and only ion current is collected at the anode. The ions contributing to the ion current are formed at the tungsten surface and do not result from ionization of residual gas in the system. The ion current is present at slightly smaller negative anode voltages, and the 4-6 v electrons do not have enough energy to ionize gas atoms present in the vacuum chamber. There will be too few electrons of higher energy to effect ionization at the operating pressure. The occurrence of these ions at the tungsten surface is therefore further evidence of very high surface temperatures, for this implies thermal ionization of atoms or molecules at this surface. The question which now arises is whether these ions are derived from adsorbed gases at the tungsten surface or from the tungsten itself. This has not been answered conclusively, although the scanty evidence available would indicate that they are tungsten ions. When the laser beam is first turned on, after the system has been inoperative overnight, a large current burst is observed. Subsequent shots at a timed interval give a smaller but consistent current level. Two factors would contribute to this. First, the laser housing is not forced cooled, so that upon slight average heating the output energy of the laser will drop slightly with a constant input energy. Also, gas adsorbed on the tungsten surface over

a long time interval will be blasted from the surface. The adsorbed gas is probably the principal contributor to the large current burst observed for the first laser shot, since the vacuum pressure shows a slight jump on the first burst and is almost steady for subsequent bursts. Also at the pressure of 10^{-8} Torr, there are approximately 3.9×10^{12} molecules striking a square centimeter of the cathode per second. If it is assumed that the sticking coefficient is one, and that 8.2×10^{14} molecules are required to form a monolayer on the tungsten, it would take about 3.5 minutes for this layer to form. The sticking coefficient will be less than one, however, and the brief period when the cathode surface is hot will contribute to lengthen the time required to form this monolayer. The repetition rate used for the laser was usually one burst per minute. This question of which particles take part in the ion currents should be investigated further. A simple way would be to have a lower pressure during operation.

An interesting feature of the data shown in Figure 16 for an anode voltage of -6 v is that the spiked electron current occurs in the vicinity of the ion current spikes. Thus, this current may be "carried" along with the ion current and give the appearance of large amounts of electrons with high energy. A rough indication that this occurs is given in Figure 17, which was obtained by averaging the electron current of the spikes for a sequence of applied anode voltages. These data are approximate, since the occurrence of ion bursts at the negative applied voltages makes the averaging process difficult. Although not shown in Figure 17, the electron current at larger negative voltages tends to give a flattened curve, which would be expected from the effect of the ions in partially

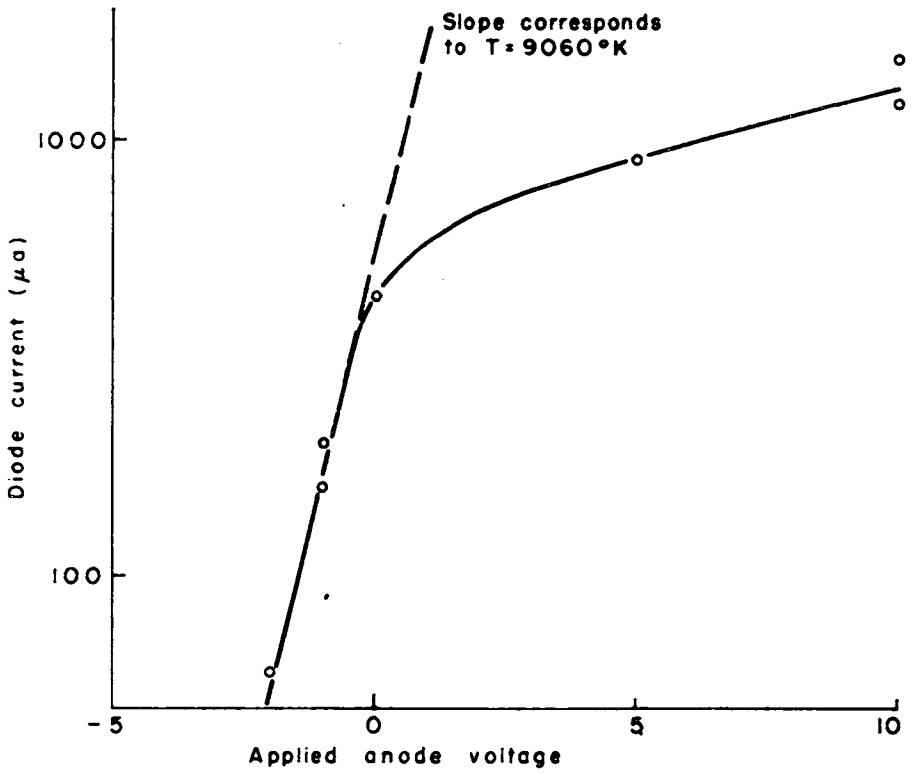

FIGURE 17. Retarded Field Plot
for Laser-induced Electron Emission.

neutralizing the applied field. Better data in this regard should be available from the second diode structure. It is interesting to observe in Figure 17 that if these data were treated as ordinary retarded-field data from a conventional diode, the slope of the curve indicates a cathode temperature of 9,000 - 10,000° K.

Some preliminary data have been taken with the second diode structure for the simultaneous emission of electrons and ions. One of the anodes had a positive voltage with respect to the cathode, whereas the other anode had a negative voltage. Small ion currents, on the order of those shown in Figure 16, were collected at the negative anode. The ion current bursts would begin near the peaks of the electron current spikes and would last for a longer period. Unfortunately, in this preliminary data, ringing occurred in the ion-current viewing circuit, so that the data were not clear and consequently are not presented here.

An example of the detailed study made of the time correlation between the electron current spikes and the laser spikes is shown in Figure 18. The phototube output is shown as the lower trace and the electron current spikes are shown in the upper trace. This figure shows the limitation of the frequency response of the phototube detector circuit. The result in Figure 18 was consistently seen in other data. i. e., for each laser spike there is a spike of electron current; therefore, there is a time correlation between the occurrence of a laser spike and a current spike. Apparently, however, there is no amplitude correlation between these two sets of spikes, as shown in Figure 19 and 20 where the lower trace is the phototube output. Here the electron current scale has been compressed as compared to Figure 18 so that very low-level current spikes are not visible. The two photographs in Figure 20 were taken with a large laser output, whereas the two in

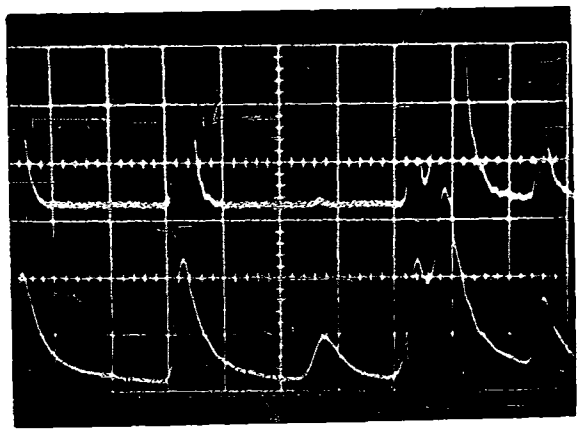

FIGURE 18. Typical Data Sample, Showing Occurence of Electron Emission Spike for Each Laser Spike, Top Trace Is Current. Current Scale: 500 μa/div., Time Scale: 1 μs/div.

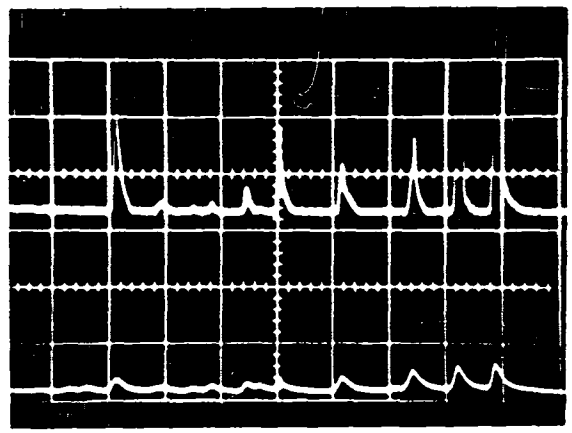

(a)

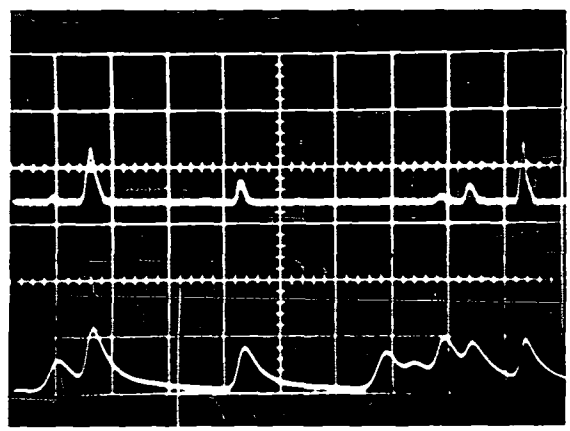

(b)

FIGURE 19. Time Correlation between Electron Emission Current and Laser Spikes at Low Current Levels. Anode Voltage: 500 v Positive for All Data. (a) Current Scale: 500 μa/div., Time Scale: 2 μs/div.; (b) Current Scale: 500 μa/div., Time Scale: 1 μs/div.

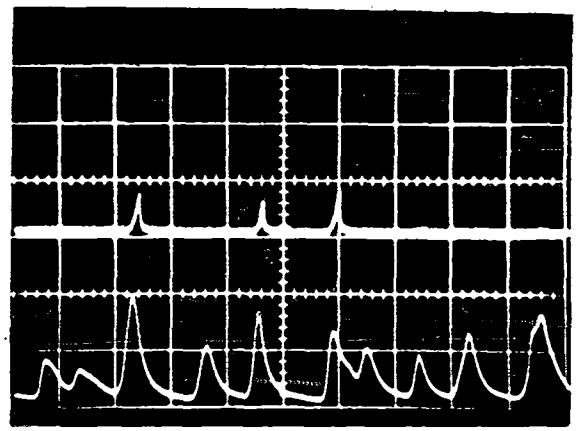

(a)

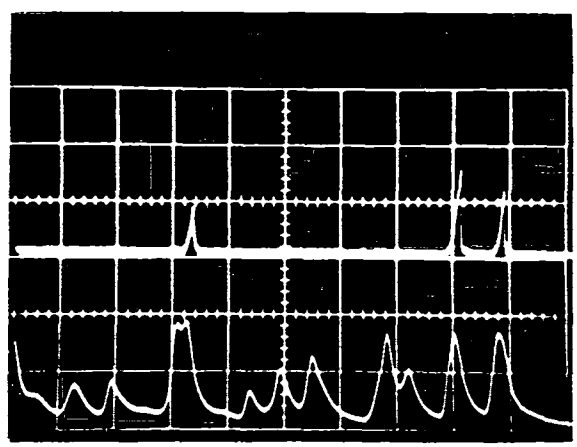

(b)

FIGURE 20. Time Correlation at High Current Levels.
(a) Current Scale: 100 ma/div., Time Scale: 2 μs/div.;
(b) Current Scale: 50 ma/div., Time Scale: 2 μs/div.

Figure 19 were taken with a small laser output within the range of 0.13 to 0.62 joules incident on the cathode surface noted earlier. From these data, it is apparent that the current spikes have a delay of several tenths of a microsecond with respect to the laser spikes at the larger laser energies. In addition, even though the same circuitry was used for these four photographs, the fall times of the current spikes for the larger laser energies were significantly shorter than those for the small laser energies. This could be related to the emission of ions which occurs near the peak of the electron current at the high laser levels and which would tend to cool the surface.

The reason for the lack of amplitude correlation between the electron and laser spikes is not known. Possible explanations are that occluded gases near the surface, especially hydrogen may affect the work function of the spots from laser spike to spike, or that the illuminated area varies from spike to spike. The second explanation appears more likely than the first, since one would expect that any gas absorbed near the surface of the tungsten would be released after several laser bursts, and reabsorption is a long-term process. Certainly gas adsorption on the surface is not important in the short time scale between spikes in one laser burst; but if the pulsed laser tends to operate in a different spatial mode for each output spike, then a different degree of divergence associated with each spike would result in a different area being illuminated.

From previous data, a change in incident energy of five to one changes the emission current by approximately 10^6; therefore, a change in the effective area of 50 - 100 per cent would easily render the resultant current pulse undetectable on the linear scale used in recording the diode current.

An examination of average electron-emission current during the laser burst was made by using a nonlinear viewing circuit for the diode current. This circuit is shown in Figure 21 and data samples are shown in Figure 22. In Figure 22, the bottom photograph is taken for a larger bias voltage for the diode, so that the current spikes are visible in relation to the average emission current. A careful check of the measuring circuit showed that the indicated average current actually occurs; i. e., it is not due to partial rectification of the electron current spikes in the viewing circuit. Note that the peak magnitude of the spiked current is approximately one thousand times larger than the average current and that the average current dies rapidly during the laser burst. This appears to coincide with the laser output being most intense near the beginning of the burst in Figure 22.

Qualitatively, most of the results seen in the thermionic emission of electrons were predicted by the simple classical theory described in Chapter II. The electron emission current occurs predominantly in spikes that tend to follow the laser spikes with a slight time delay, as indicated by Figures 3 and 4. Also, the surface temperature appears to follow the laser pulses surprisingly well. Although it is surprising that the temperature changes so rapidly,

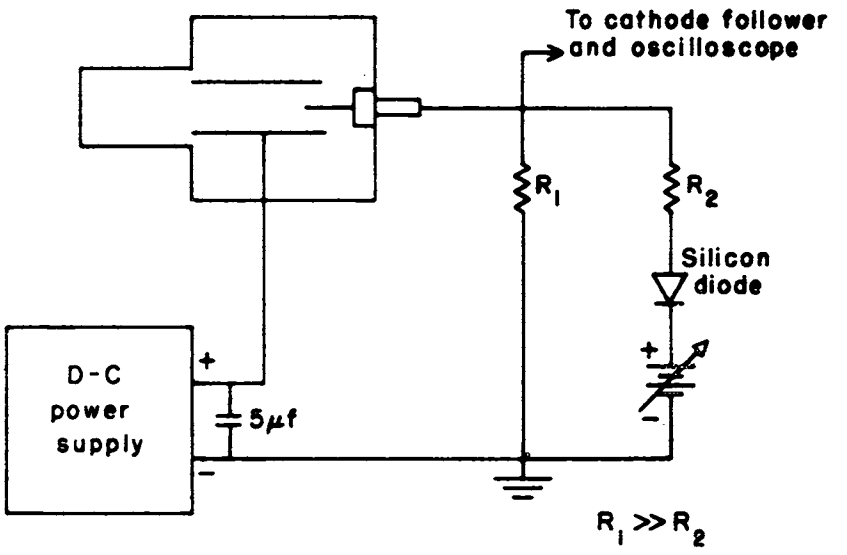

FIGURE 21. Typical Circuit Used to Automatically Switch Current Sensitivity on Oscilloscope.

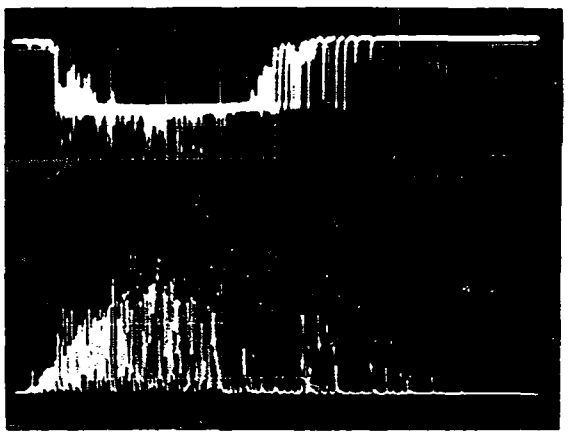

(a)

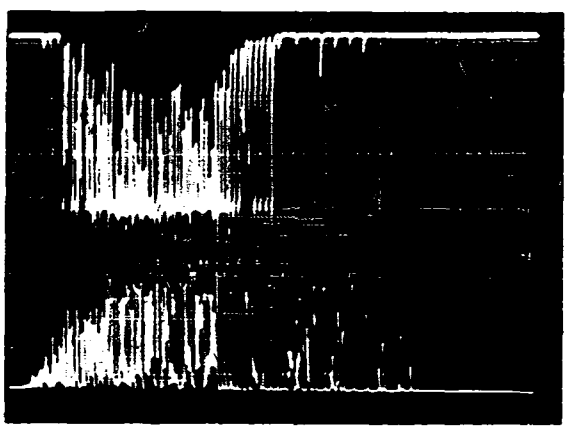

(b)

FIGURE 22. Typical Data Showing Average Emission Current during Laser Burst, Using Circuit Shown in Figure 18. Anode: 500 v Positive with Respect to Cathode. (a) Current Scale: 100 μa/div. for 1 div., and 100 ma/div. above 1 div., Time Scale: 50 μs/div.; (b) Current Scale: 50 μa/div. for 3 div., and 50 ma/div. above 3 div.; Time Scale: 50 μs/div.

the rapid change becomes reasonable if one realizes that a very large energy is deposited into a very small volume near the surface of the cathode. That the loss of material from the cathode surface is small, even though high peak temperatures are involved, is indicated by a visual examination of the surface after repeated bombarding and by the small ion currents observed at negative anode voltages. One of the test conditions that helps to reduce the loss of material is the collection of emission current only on a single positive anode. The applied field would tend to push any ions generated at the cathode back to the cathode surface, where they would be neutralized. No data are presently available on loss of material for extended emission tests, where ions and electrons are collected separately in the second diode structure.

It is interesting that the approximate theoretical prediction of the surface temperature is of the same order of magnitude as that obtained from the retarded-field plot in Figure 17. The very high peak emission-current densities result from the high instantaneous temperature at the surface and, possibly, from a photoemission effect, as discussed in Section II F. There is no evidence of an ion cloud in front of the cathode, which would tend to give a high electric field at the cathode surface and, therefore, result in some field emission as claimed by other workers[2, 3]. In preliminary tests with the second diode structure, high electron emission was still observed even when ions were swept away from the cathode with a large negative potential (900 v) on one of the anodes. The simple theory presented earlier does not account for this emission of ions, nor does it account for the cooling effects of this emission.

Finally, the average emission current observed during a laser burst would be predicted theoretically by extending the estimate for the emission current in Figures 3 and 4 to lower current levels. Such a calculation, however, would predict an average emission current lasting at least to the end of the laser burst, which was not observed experimentally, although it is possible that the current-measuring sensitivity was not high enough near the end of the laser burst.

2. Ion Emission

Typical data showing the emission of small ion currents are shown in Figures 23 and 24. This emission, as for the case included in Figure 16, is obtained by operating the laser at an output energy approximately equal to that required for the maximum thermionic emission. Some interesting but unexplained differences in the ion emission are apparent in the data shown in Figures 23 and 24. In Figure 23 a ,, the emission was obtained from the first diode structure with an anode voltage of -500 v with respect to the cathode. The width of the base line of the ion burst is from 5 to 10 μs. In Figures 23 b and 24 a, the emission was obtained from the second diode structure by connecting both anodes together at the common potential of 300 v negative with respect to the cathodes. Here, the width of the base line of the ion bursts is approximately 2 μs. For Figure 24 b, one anode in the second diode structure was used to collect ion current at -300 v, while the other anode was connected directly to the cathode. For this case the ion pulses are from 5 to 10 μs long at the

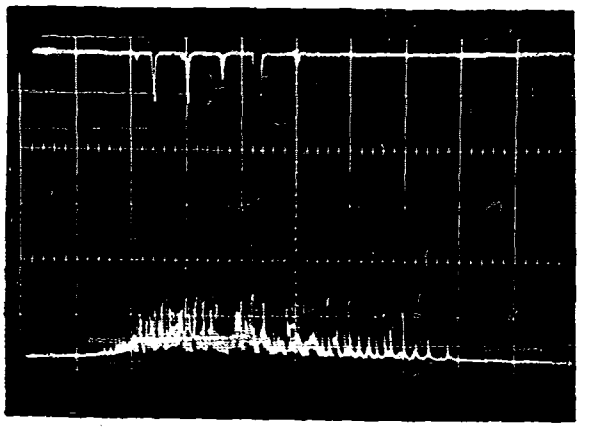

(a)

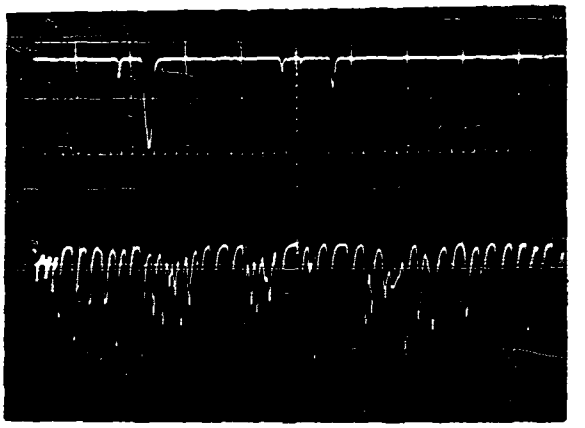

(b)

FIGURE 23. Emission of Small Ion Currents; Lower Trace Is Laser Output for All Data. (a) Anode: 250 v Negative with Respect to Cathode, Current Scale: 200 μa/div., Time Scale: 50 μs/div.; (b) Anode: 300 v Negative with Respect to Cathode, Current Scale: 200 ma/div., Time Scale: 50 ms/div.

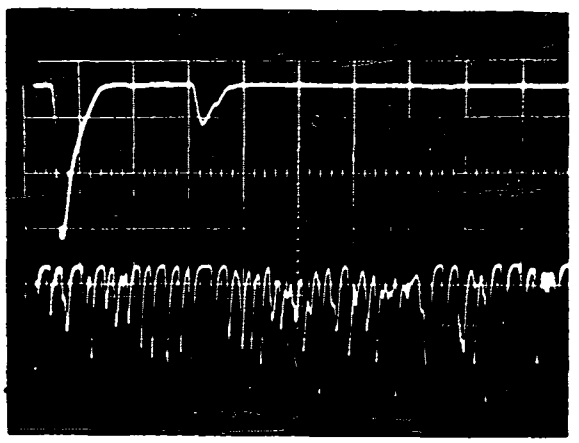

(a)

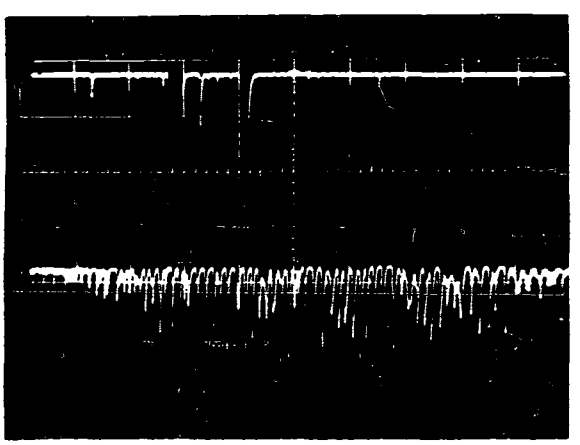

(b)

FIGURE 24. Emission of Small Ion Currents, Lower Trace Is Laser Output for All Data. (a) Anode: 300 v Negative with Respect to Cathode, Current Scale: 200 μa/div., Time Scale: 20 μs/div.; (b) Anode: 300 v Negative with Respect to Cathode, Current Scale: 200 μa/div. Time Scale: 10 μs/div.

base line. Different times of flight are probably not causing a difference in the observed pulse widths, at least for the case shown in Figure 24b. Here, the trailing edge of the ion pulses reminds one of the frequency-response limitations of the circuit, although why the poor time response results from simply connecting one of the anodes to the cathode is not known. A further investigation of this is required.

When the laser output energy is increased by a factor of 2 to 2.5 times that used to obtain the data in Figure 24, a much larger emission of ion current than that shown in Figure 24 results when the anode is negative with respect to the cathode. Some of the typical data obtained are shown in Figures 25 and 26. For this data, a dual-beam oscilloscope was not used, so only the diode current is shown as a function of time. It is seen that the peak diode current in Figures 25 and 26 ranges from several amperes to over 30 a. This emission proved to be somewhat erratic, since the same laser output energy would often give very different results in terms of ion emission. Also, the surface of the tungsten cathode was very badly eroded whenever these large ion currents were drawn from the cathode. It is apparent, then, that this ion current consists largely of tungsten ions resulting from thermal ionization of tungsten atoms at the cathode surface. Accompanying this ion current, the pressure in the diode showed a jump of approximately one-half an order of magnitude; i.e., if the initial pressure was 1×10^{-8} Torr, the pressure would jump to 5×10^{-8} Torr, and then gradually settle to its original value. This jump in pressure could be accounted for by gas atoms or molecules,

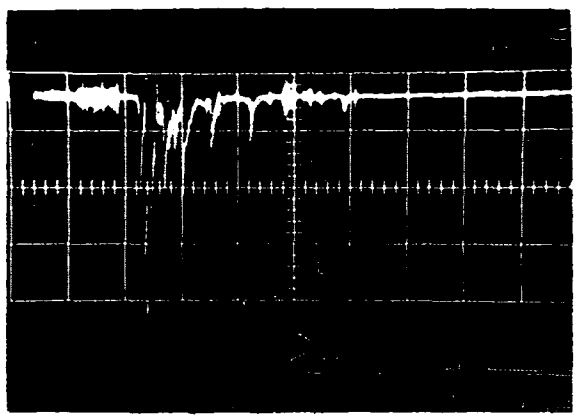

(a)

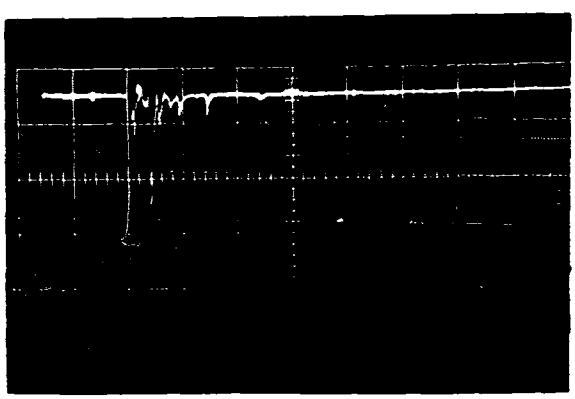

(b)

FIGURE 25. Emission of Large Ion Currents, (a) Current Scale: 200 ma/div., Time Scale: 50 μs/div.; (b) Current Scale: 500 ma/div., Time Scale 50 μs/div.

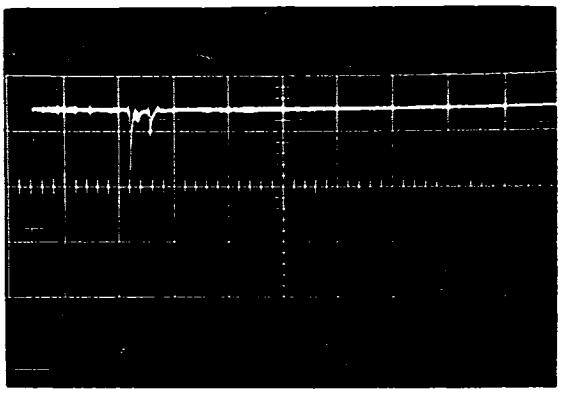

(a)

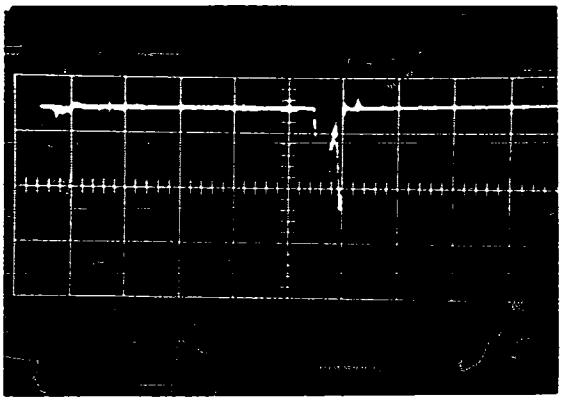

(b)

FIGURE 26. Emission of Large Ion Currents, (a) Current Scale: 2 a/div., Time Scale: 50 μs/div.; (b) Current Scale: 10 a/div., Time Scale: 50 μs/div.

occluded in the cathode material, being released by the large cathode erosion. No other data for this type of emission are shown, because the emission of large ion currents was not investigated intensively.

3. Plasma Discharge

When the laser output energy is increased very slightly above that required for the maximum thermionic emission and the anode of the diode is positive with respect to the cathode, a type of plasma discharge occurs. Illustrative data for this are shown in Figures 27 and 28. The laser energy incident on the cathode surface was approximately 0.8 joules for the data shown. In these figures, the lower trace is the diode voltage; the upper trace is the diode current, where a downward deflection indicates electron current collected at the anode or ion current collected at the cathode. It is observed that when a plasma discharge occurs, the diode voltage drops to a low value, 10 to 20 v, and the total diode current is determined by the circuit resistance and supply voltage minus the voltage drop of the diode. For these data, an additional capacitor bank of 2000 μf was added in parallel to that shown attached to the power supply in Figure 10. This capacitor bank supplied the large peak current drawn by the diode, which is shown in Figures 27 and 28.

When a relatively low peak-diode current is drawn, on the order of 5 to 10 a, the diode current is erratic in time and very noisy, as shown in Figure 27. In addition, when the laser beam is turned off, the diode current ceases. Under the same operating conditions, however, except with a smaller circuit resistance, the

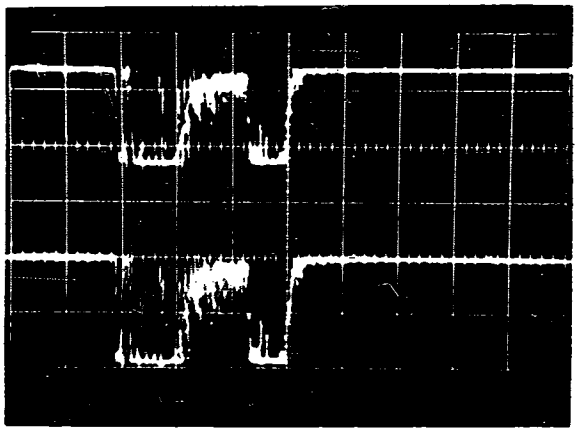

(a)

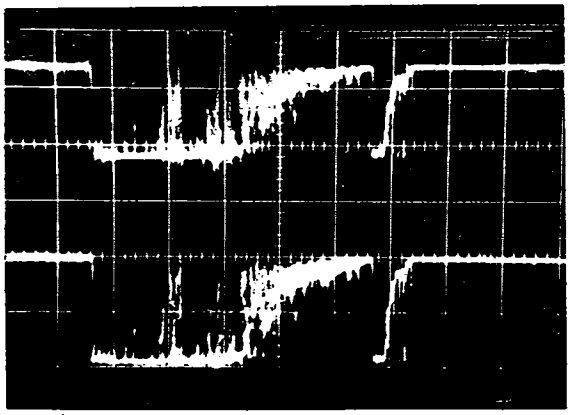

(b)

FIGURE 27. Diode Current and Voltage for Plasma Discharge. Anode Supply Voltage: 400 v Positive with Respect to Cathode. Lower Trace Is Diode Voltage with Scale of 200 v/div. (a) Current Scale: 4.5 a/div., Time Scale: 50 μs/div.; (b) Current Scale: 5 a/div., Time Scale: 50 μs/div.

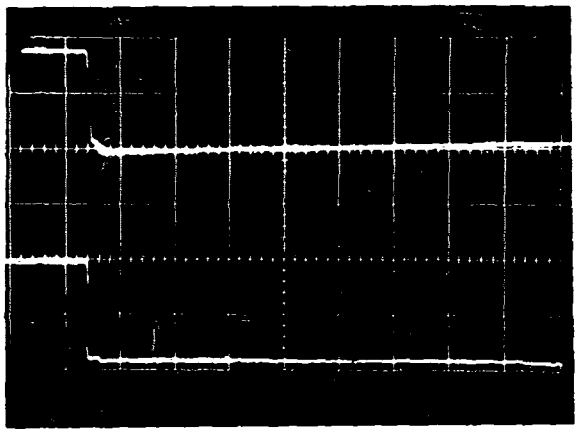

(a)

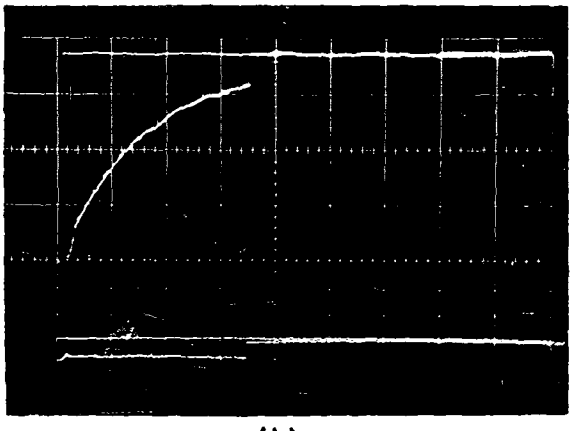

(b)

FIGURE 28. Diode Current and Voltage for Plasma Discharge. Anode Supply Voltage; 400 v Positive with Respect to Cathode. Lower Trace Is Diode Voltage with Scale of 200 v/div. (a) Current Scale: 150 a/div., Time Scale: 50 μs/div.; (b) Current Scale: 20 a/div., Time Scale: 10 ms/div.

plasma discharge, once initiated by the laser beam, lasts well beyond the time the laser beam turns off. This is illustrated in Figure 28 a and, especially, Figure 28 b, where the discharge is seen to last for at least 100 times the length of the laser beam. The decay, visible in the diode current in Figure 28 b, is simply the RC discharge characteristic of the circuit capacity and resistance. In addition to lasting for a relatively long time at the higher current levels, the plasma discharge is also very quiet compared to the lower current levels.

For the short-duration plasma discharge at low current levels, the laser beam will blast neutral atoms or particles, electrons, and ions from the surface. Electrons are accelerated towards the anode and collide with neutral particles, producing more electrons; and the discharge builds up in the usual way. The interesting feature is that the gas being ionized in this instance is produced from the vaporization of the cathode and is probably composed largely of tungsten atoms. The ions return to the cathode surface, but the current is not large enough for the discharge to be self-sustaining. A typical pressure jump in the vacuum system for this mode of operation may be from 10^{-8} Torr to 5×10^{-7} Torr.

The long-duration plasma discharge at high current levels is initiated in the same way as the short-duration discharge. Now, however, the current is high enough for the discharge to sustain itself. In the brief investigation made of this phenomenon, it was not clear why the discharge maintained itself. The pressure in the diode rose rapidly, and at the time the discharge stopped, the ion pump would often shut itself off because of the very large gas burst that occurred.

This gas was probably released both from the cathode by the returning ions and from the anode by the bombardment with the heavy electron current. Thus, after this discharge was initiated, gas atoms were probably playing as large a part in the discharge, if not larger, than the tungsten atoms. This phenomenon should be investigated at much lower operating pressures, especially with the diode structure well outgassed.

When the laser output energy was increased so that it approached 2 to 3 joules incident on the cathode surface, and when the anode was held at a negative potential with respect to the cathode, another type of long-term plasma discharge occurred. This discharge was also accompanied by a large pressure burst and a relatively low diode voltage. A possible mechanism for this discharge is that an ion current is initiated that is sufficiently large to produce enough electrons from the copper anode to sustain the discharge. The gas released from the diode structure would probably also play a major role in sustaining the discharge after the laser pulse has ceased.

An interesting observation in the plasma discharge from the tungsten cathodes is the very high electron density associated with the large discharge current. For an estimate of the order of magnitude of the plasma frequency that can occur, observe that the peak current is approximately 260 a in Figure 23a. If one assumes that a short distance in front of the cathode, the discharge plume is approximately 10-mil in diameter, that the electron current is 100 a. and that the electron velocity is 2×10^6 m/s (approximately 10v); then one calculates a plasma frequency of about 800 Gc/s. This rough calculation indicates that this plasma discharge may have an important application in the generation of submillimeter waves.

4. Heated Tungsten Cathode

The tungsten wire cathode in the second diode structure was directly heated by passing a current through the wire. Under these conditions, a focused laser beam illuminated a small portion of the side of the wire and the laser-induced current was measured with the apparatus shown in Figure 10. A summary of the preliminary results of this experiment is shown in Figure 29. Individual traces of the diode current revealed the spiked structure shown in previous figures. The curve labeled "average spike current" represents an average of the amplitudes of all current spikes taken over the duration of the laser burst. The other curve represents the highest current spike during the laser burst. Care was taken to maintain the laser output energy constant for the series of shots comprising these data by firing the laser at timed intervals. Both anodes and grids in the diode were electrically connected and were 500 v positive with respect to the cathode. Unfortunately, the operating pressure was rather high for the results shown, probably because the hot tungsten filament was heating the epoxy glue holding the grid structure to the anode. Consequently, the pressure ranged from 4×10^{-6} Torr to 3×10^{-7} Torr during the tests. The greatest pressure rise occurred near the knee of the curve in Figure 29, so that ionization of the gas present is undoubtedly playing a role in the sharp increase in current observed as a function of cathode temperature. Further tests are required before one can say with certaintly that a hot tungsten cathode will give a higher laser-induced electron emission than a cold tungsten cathode.

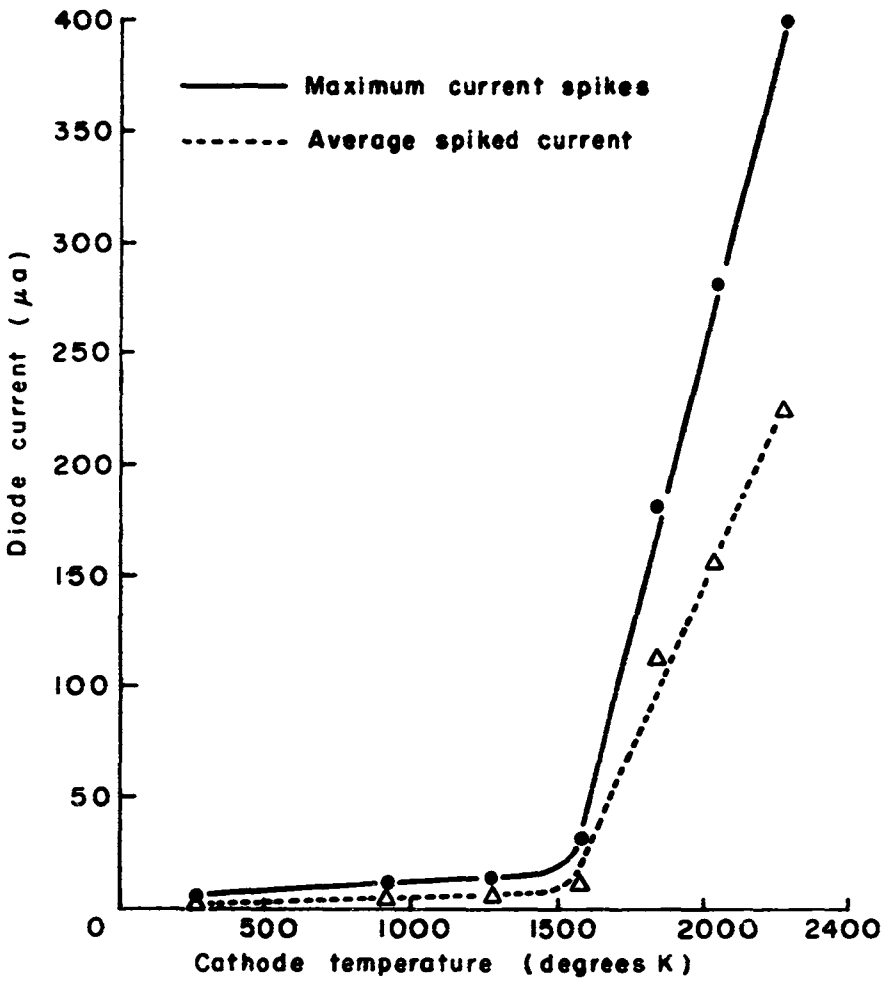

FIGURE 29. Preliminary Data on Laser-induced Emission from a Hot Tungsten Cathode.

IV. CONCLUSIONS AND RECOMMENDATIONS FOR FURTHER WORK

A. CONCLUSIONS

The principal conclusions from this study of laser-induced emissions are as follows:

1. The electron emission density obtained when a focused laser beam heats the surface of a tungsten cathode is larger than had been anticipated. The conservative estimate of 10^4 a/cm^2 is an order of magnitude larger than originally estimated.

2. The simple classical theory derived in this report is adequate to describe the electron emission obtained from a tungsten cathode, qualitatively.

3. A plasma discharge having an extraordinarily high plasma frequency can be induced from a tungsten target by a focused laser beam.

4. Emission of ion currents on the order of amperes is possible by using a focused laser beam to illuminate a tungsten target. This should work as well with other metallic targets and is a good possible source of high-density ion beams.

B. RECOMMENDATIONS FOR FURTHER WORK

Future work in this area should be directed toward two major objectives. The first is the investigation of devices utilizing the laser-induced emission. Such devices would include the formation

of the electron emission into a small, high-density electron beam for application to millimeter-wave beam tubes. Another possibility is the harnessing of the plasma discharge to provide signal generators or amplifiers at millimeter and submillimeter wavelengths. A third possibility is the formation of a high-density ion-beam source.

The second principal objective of further work should be an understanding of the mechanisms involved in the phenomena described. Although a general description has been made of most of the observed events, no detailed knowledge of just how these events occur is given, nor is it known. A necessary step in this direction will be the formulation of a more precise theory based on quantum mechanics, which will undoubtedly suggest further experimental work in addition to experimental work now in progress.

V. REFERENCES

1. G. J. Wolga and C. A. Waterstrat, "Improved Procedure for Fabrication of High-Efficiency Laser Cavities," submitted to Rev. Sci. Inst. for publication.

2. R. E. Honig and J. R. Woolston, "Laser Induced Emission of Electrons, Ions, and Neutral Atoms from Solid Surfaces," Appl. Phys. Letters, 2 (April 1963), pp. 138-139.

3. David Lichtman and J. F. Ready, "Laser Beam Induced Electron Emission," Phys. Rev. Letters, 10 (April 1963), pp. 342-345.

UNCLASSIFIED